Impacts of seawater saturation state ($\Omega_A = 0.4–4.6$) and temperature (10, 25 °C) on the dissolution kinetics of whole-shell biogenic carbonates

Justin B. Ries [a,*], Maite N. Ghazaleh [b,c], Brian Connolly [b], Isaac Westfield [a], Karl D. Castillo [b]

[a] *Department of Marine and Environmental Sciences, Northeastern University, Nahant, MA 01908, United States*
[b] *Department of Marine Sciences, University of North Carolina at Chapel Hill, Chapel Hill, NC 27514, United States*
[c] *Department of Environmental Health Science, University of Georgia, Athens, GA 30602, United States*

Received 21 July 2015; accepted in revised form 5 July 2016; available online 14 July 2016

Abstract

Anthropogenic increase of atmospheric pCO_2 since the Industrial Revolution has caused seawater pH to decrease and seawater temperatures to increase—trends that are expected to continue into the foreseeable future. Myriad experimental studies have investigated the impacts of ocean acidification and warming on marine calcifiers' ability to build protective shells and skeletons. No studies, however, have investigated the combined impacts of ocean acidification and warming on the whole-shell dissolution kinetics of biogenic carbonates. Here, we present the results of experiments designed to investigate the effects of seawater saturation state ($\Omega_A = 0.4–4.6$) and temperature (10, 25 °C) on gross rates of whole-shell dissolution for ten species of benthic marine calcifiers: the oyster *Crassostrea virginica*, the ivory barnacle *Balanus eburneus*, the blue mussel *Mytilus edulis*, the conch *Strombus alatus*, the tropical coral *Siderastrea siderea*, the temperate coral *Oculina arbuscula*, the hard clam *Mercenaria mercenaria*, the soft clam *Mya arenaria*, the branching bryozoan *Schizoporella errata*, and the coralline red alga *Neogoniolithon* sp. These experiments confirm that dissolution rates of whole-shell biogenic carbonates decrease with calcium carbonate ($CaCO_3$) saturation state, increase with temperature, and vary predictably with respect to the relative solubility of the calcifiers' polymorph mineralogy [high-Mg calcite (mol% Mg > 4) ≥ aragonite > low-Mg calcite (mol% Mg < 4)], consistent with prior studies on sedimentary and inorganic carbonates. Furthermore, the severity of the temperature effects on gross dissolution rates also varied with respect to carbonate polymorph solubility, with warming (10–25 °C) exerting the greatest effect on biogenic high-Mg calcite, an intermediate effect on biogenic aragonite, and the least effect on biogenic low-Mg calcite. These results indicate that both ocean acidification and warming will lead to increased dissolution of biogenic carbonates in future oceans, with shells/skeletons composed of the more soluble polymorphs of $CaCO_3$ being the most vulnerable to these stressors. The effects of saturation state and temperature on gross shell dissolution rate were modeled with an exponential asymptotic function ($y = B_0–B_2 \cdot e^{B_1\Omega}$) that appeals to the general Arrhenius-derived rate equation for mineral dissolution [$r = (C \cdot e^{-E_a/RT})(1 - \Omega)^n$]. Although the dissolution curves for the investigated biogenic $CaCO_3$ exhibited exponential asymptotic trends similar to those of inorganic $CaCO_3$, the observation that gross dissolution of whole-shell biogenic $CaCO_3$ occurred (albeit at lower rates) even in treatments that were oversaturated ($\Omega > 1$) with respect to both aragonite and calcite reveals fundamental differences between the dissolution kinetics of whole-shell biogenic $CaCO_3$ and inorganic $CaCO_3$. Thus, applying stoichiometric solubility products derived for inorganic $CaCO_3$ to model gross dissolution of biogenic carbonates may substantially underestimate the impacts of ocean acidification on net calcification (gross calcification minus gross

* Corresponding author at: 430 Nahant Road, Nahant, MA 01908, United States.
E-mail address: j.ries@neu.edu (J.B. Ries).

http://dx.doi.org/10.1016/j.gca.2016.07.001

dissolution) of systems ranging in scale from individual organisms to entire ecosystems (e.g., net ecosystem calcification). Finally, these experiments permit rough estimation of the impact of CO_2-induced ocean acidification on the gross calcification rates of various marine calcifiers, calculated as the difference between net calcification rates derived empirically in prior studies and gross dissolution rates derived from the present study. Organisms' gross calcification responses to acidification were generally less severe than their net calcification response patterns, with aragonite mollusks (bivalves, gastropods) exhibiting the most negative gross calcification response to acidification, and photosynthesizing organisms, including corals and coralline red algae, exhibiting relative resilience.

Keywords: Dissolution kinetics; Ocean acidification; Global warming; Gross calcification; Gross dissolution; Net calcification; Calcium carbonate; Marine calcifier; Calcareous organism

1. INTRODUCTION

Daily mean atmospheric carbon dioxide (pCO_2) exceeded 400 ppm at the Mauna Loa (Hawaii) observatory in May 2013 (Tans and Keeling, 2013), an approximate 43% increase from the pre-Industrial-Revolution level of 280 ppm (IPCC, 2013). This increase in atmospheric pCO_2 has caused surface seawater pH to decline by approximately 0.1 units (Brewer, 1997; Caldeira and Wickett, 2003; Orr et al., 2005; IPCC, 2013) and surface seawater temperatures to increase by approximately 1 °C (Kleypas et al., 2005; IPCC, 2013). Atmospheric pCO_2 is predicted to increase to between 700 and 900 ppm by the end of the 21st century, which should cause sea surface pH to decrease by an additional 0.3–0.4 units (Brewer, 1997; Caldeira and Wickett, 2003; Orr et al., 2005; Raven et al., 2005; Füssel, 2009; Egleston et al., 2010; IPCC, 2013) and surface seawater temperatures to increase by 2–4 °C (Eakin et al., 2008; Donner, 2009; IPCC, 2013) over the same timeframe. This decrease in seawater pH will reduce the seawater concentration of carbonate ions ($[CO_3^{2-}]$), which marine calcifiers use to build their calcium carbonate ($CaCO_3$) shells and skeletons.

Myriad experimental studies (too numerous to mention here) have demonstrated that CO_2-induced ocean acidification impairs calcification within many species of marine calcifiers. Review articles by Kleypas et al. (1999, 2005), Langdon (2002), Hoegh-Guldberg et al. (2007), Fabry et al. (2008), Doney et al. (2009), Hendricks et al. (2010), and Kroeker et al. (2013) provide excellent summaries of the many studies conducted to date. Several studies also suggest that calcification within some species of marine calcifiers is not negatively impacted and, in some cases, is actually enhanced by moderate elevations in atmospheric pCO_2 (e.g., Iglesias-Rodriguez et al., 2008; Wood et al., 2008; Ries et al., 2009; Rodolfo-Metalpa et al., 2010, 2011; Fabricius et al., 2011; Castillo et al., 2014).

The process of shell-building (i.e., 'net calcification') within marine calcifiers inhabiting near-undersaturated waters results from the balance of forming new shell through active calcification (i.e., 'gross calcification') and losing old shell through dissolution (i.e., 'gross dissolution'; e.g., Ries, 2011a, 2012; Rodolfo-Metalpa et al., 2011). Benthic marine calcifiers inhabiting restricted coastal waters can experience seawater pCO_2 that is higher than equilibrium pCO_2 for surface seawater in the open ocean due to seasonal cycles in the respiration of organic carbon and/or upwelling and/or water mixing (e.g., Feely et al., 2008; Andersson and Mackenzie, 2012; Andersson and Gledhill, 2013). Calcifiers inhabiting these restricted coastal environments are already experiencing seawater that is undersaturated or nearly undersaturated with respect to their shell mineralogy, which supports the gross dissolution of existing shell (either exposed, distal to calcifying tissue, and possibly covered by calcifying tissue; e.g., Andersson et al., 2005, 2006, 2008, 2011; Morse et al., 2006; Andersson and Mackenzie, 2012; Andersson and Gledhill, 2013) and biologically mediated gross calcification beneath healthy calcifying tissue (e.g., Wood et al., 2008; Ries et al., 2009; Ries, 2011a; Rodolfo-Metalpa et al., 2010, 2011; Fabricius et al., 2011). Furthermore, this dissolution of biogenic carbonates is predicted to increase by more than 200% by year 2300 under business-as-usual scenarios (Kleypas et al., 2005; Andersson et al., 2005, 2006, 2008, 2011; Morse et al., 2006; IPCC, 2013; Andersson and Mackenzie, 2012; Andersson and Gledhill, 2013; Pickett and Andersson, 2015).

Although numerous studies have investigated the impact of CO_2-induced ocean acidification on organisms' rates of net calcification (gross calcification minus gross dissolution), relatively few studies have endeavored to isolate the effects of ocean acidification on the gross dissolution (e.g., Morse et al., 1979; Keir, 1980; Kennish and Lutz, 1999; Cubillas et al., 2005; Bednaršek et al., 2012; Pickett and Andersson, 2015) or gross calcification (e.g., Comeau et al., 2010; Rodolfo-Metalpa et al., 2011; Cohen and Fine, 2012) of marine calcifiers' shells and skeletons. And none has investigated the combined impacts of warming and acidification on these processes. Indeed, it is presently unclear which of these two processes (gross dissolution vs. gross calcification) is most directly impacted by ocean acidification (e.g., Andersson et al., 2008, 2011; Ries et al., 2009; Ries, 2011a, 2012; Rodolfo-Metalpa et al., 2011; Andersson and Gledhill, 2013; Pickett and Andersson, 2015).

Here we present the results of 47-day laboratory experiments investigating the independent and combined effects of seawater saturation state ($\Omega_A = 0.4$–4.6) and temperature (10, 25 °C) on rates of whole-shell gross dissolution for 10 species of marine calcifiers that span a range of carbonate polymorph mineralogies (low-Mg calcite, high-Mg calcite, and/or aragonite): the oyster *Crassostrea virginica*, the ivory barnacle *Balanus eburneus*, the blue mussel

Mytilus edulis, the conch *Strombus alatus*, the tropical coral *Siderastrea siderea*, the temperate coral *Oculina arbuscula*, the hard clam *Mercenaria mercenaria*, the soft clam *Mya arenaria*, the branching bryozoan *Schizoporella errata*, and the coralline red alga *Neogoniolithon* sp. Gross calcification rates for a subset of these species are also roughly estimated from the difference between their previously determined net calcification rates (Ries et al., 2009; Castillo et al., 2014) and their empirically derived gross dissolution rates (this study).

1.1. Overview of prior work on the dissolution kinetics of $CaCO_3$

The dissolution kinetics of calcium carbonate minerals comprise a vast body of theoretical and empirical research that has now been explored for more than half a century. The field has received such widespread attention because of its relevance to a broad range of industries and scientific disciplines. Industrial applications relevant to $CaCO_3$ dissolution include antifouling of marine and freshwater structures (e.g., turbines, boat hulls), descaling of pipes and industrial reactors, art conservation, ceramics, dentistry, vascular and soft-tissue decalcification, mineralogical sequestration of fossil-fuel derived CO_2, the development of oil and gas reservoirs, and the mineralogical sealing of oil and gas wells. Calcium carbonate dissolution is also relevant to countless scientific subjects, including the global carbon cycle, sedimentary diagenesis, the formation, abundance and distribution of limestones, the evolution of ocean chemistry, fossil preservation, lysocline dynamics, buffering of the seawater carbonate system, and the biological and sedimentary responses to ocean acidification and warming. Because many natural waters exist near the $CaCO_3$ precipitation–dissolution divide, the $CaCO_3$–CO_2–H_2O system has become a model for the empirical exploration of mineral dissolution kinetics.

Although a thorough review of prior studies investigating the dissolution kinetics of $CaCO_3$ minerals is beyond the scope of the present contribution, a brief overview of the field is presented below. Readers seeking a more comprehensive treatment of the subject are directed to reviews by Plummer et al. (1979), Morse (1983), Mackenzie et al. (1983), Morse and Mackenzie (1990), Morse and Arvidson (2002), Morse et al. (2006, 2007), and Andersson and Gledhill (2013).

The majority of studies investigating the dissolution kinetics of $CaCO_3$ minerals have focused on synthetic carbonates, primarily calcite (Berner and Morse, 1974; Berner, 1978; Amrhein et al., 1985; Baumann et al., 1985; Busenberg and Plummer, 1986; Arakaki and Mucci, 1995; Alkattan et al., 1998; Arvidson et al., 2003; Arvidson and Luttge, 2010; Chou et al., 1989; Compton et al., 1989; Compton and Pritchard, 1990; Compton and Unwin, 1990; Dreybrodt, 1981; Dreybrodt and Buhmann, 1991; Dreybrodt et al., 1996; Finneran and Morse, 2009; Garrels et al., 1960; Garrels and Wollast, 1978; Gledhill and Morse, 2004, 2006a,b; Lafon, 1978; He and Morse, 1993; Kralj and Brečević, 1995; Gutjahr et al., 1996; Hales and Emerson, 1996; Liu and Dreybrod, 1997; Morse and Berner, 1972; Morse et al., 1979; Plath et al., 1980; Plummer and Busenberg, 1982; Plummer and Wigley, 1976; Plummer et al., 1978; Pokrovsky et al., 2005, 2009; Pokrovsky and Schott, 1999, 2002; Sjöberg and Rickard, 1984; Schott et al., 2009; Sjöberg, 1976, 1978; Svensson and Dreybrodt, 1992; Thorstenson and Plummer, 1977, 1978; Walter and Morse, 1985; Weyl, 1958, 1965; Wollast and Reinhard-Derie, 1977; Wollast, 1990; Xu et al., 2012; Bertram et al., 1991; Bischoff, 1998; Casey and Sposito, 1992). These studies generally support the theoretical assertions that the rate of $CaCO_3$ mineral dissolution can be reliably modeled by the general equation for mineral dissolution rate (cf. Morse and Arvidson, 2002; Gledhill and Morse, 2004, 2006a,b):

$$r = k \cdot (1 - \Omega)^n,$$

where r = surface-area-normalized dissolution rate, k = a rate constant, Ω = saturation state of the solution with respect to the $CaCO_3$ mineral of interest, and n = reaction order. The rate constant of the reaction (k) can be modeled from the Arrhenius equation (cf. Morse and Arvidson, 2002; Gledhill and Morse, 2004, 2006a,b) as:

$$k = C \cdot e^{-E_a/RT},$$

where C = a pre-exponential factor, E_a = Arrhenius activation energy of the reaction, R = gas constant, and T = absolute temperature (Kelvin).

Other empirical studies have shown that the dissolution kinetics of synthetic $CaCO_3$ minerals can also be influenced by a range of factors not included in the general equation for mineral dissolution rate, such as inorganic impurities (Garrels et al., 1961; Akin and Lagerwerff, 1965; Berner, 1967; Nestaas and Terjesen, 1969; Mucci and Morse, 1984; Morse, 1986; Buhmann and Dreybrodt, 1987; Mucci et al., 1989; Gutjahr et al., 1996; Eisenlohr et al., 1999; Lea et al., 2001; Alkattan et al., 2002; Arvidson et al., 2006; Harstad and Stipp, 2007; Salem et al., 1994; Terjesen et al., 1961; Walter and Hanor, 1979; Sjöberg and Rickard, 1984; Vinson and Lüttge, 2005), organic impurities (Suess, 1970; Barwise et al., 1990; Compton and Sanders, 1993; Teng and Dove, 1997), crystal surface properties (Compton et al., 1986; Schott et al., 1989; Hillner et al., 1992a,b; MacInnis and Brantley, 1992, 1993; Liang et al., 1996; Liang and Baer, 1997; Jordan and Rammensee, 1998; Shiraki et al., 2000; Lasaga and Luttge, 2001; Sjöberg and Rickard, 1984; White and Peterson, 1990; Van Cappellen et al., 1993; Teng, 2004), and ion transport adjacent to the crystal surface (e.g., Liu and Dreybrod, 1997).

A smaller body of work has investigated the dissolution kinetics of biogenic $CaCO_3$ minerals. The majority of these studies have focused on the dissolution kinetics of bulk $CaCO_3$ sediments, often with the aim of constraining reactions involved in the evolution of sedimentary porewater, early-to-late stage sedimentary diagenesis, lithification, and sedimentary buffering of the seawater carbonate system (Balzer and Wefer, 1981; Archer et al., 1989; Andersson et al., 2007, 2009; Berger, 1967; Buhmann and Dreybrodt, 1985a, 1985b; Burdige et al., 2008, 2010; Burdige and Zimmerman, 2002; Boucher et al., 1998; Friedman, 1964; Gehlen et al., 2005a, 2005b; Honjo and Erez, 1978; Hales

et al., 1994; Hales and Emerson, 1996; Jahnke and Jahnke, 2004; Kinsey, 1985; Langdon et al., 2000; Leclercq et al., 2002; Milliman, 1978; Morse, 1978; Morse et al., 2006; Peterson, 1966; Pickett and Andersson, 2015; Rude and Aller, 1991; Silverman et al., 2007a,b; Schmalz, 1965; Walter and Burton, 1990; Walter et al., 1993; Yates and Halley, 2006; Tynan and Opdyke, 2011). These studies generally investigate bulk mixtures of biogenic $CaCO_3$ minerals that, in some cases, have been substantially altered themselves through neomorphism, diagenetic conversion, laboratory cleaning, and/or natural loss of organic impurities and protective organic layers.

Numerous studies have also investigated the dissolution kinetics of specific types of biogenic $CaCO_3$ shells and skeletons (Plummer and Mackenzie, 1974; Bischoff et al., 1983, 1987; Walter and Morse, 1984, 1985; Walter, 1985; Cubillas et al., 2005). However, most of these studies involved the heavy treatment, via pulverization and/or chemical cleaning, of the shells and skeletons as the investigators sought to eliminate the effects of organic impurities, protective organic coverings, and shell and/or crystal geometry on the dissolution kinetics of the biogenic mineral (c.f., Morse and Arvidson, 2002). Although studies investigating mechanically and/or chemically treated shells and skeletons provide important insight into the dissolution kinetics of sedimentary biogenic carbonates, they are not ideal for constraining the whole-shell dissolution kinetics that are relevant to predicting organismal responses to CO_2-induced ocean acidification and warming.

Pickett and Andersson (2015) have published the most recent and comprehensive investigation of dissolution kinetics of biogenic carbonates. In their seminal study, they evaluated the impact of pCO_2 ranging from 3000 to 5500 μatm on the dissolution rates of pulverized shells of 5 species of marine invertebrates that produce calcite of varying Mg-content: a barnacle, a foraminifer, a bryozoan, an urchin, and two species of coralline algae. They found that dissolution rates increased predictably with increasing pCO_2, increasing Mg-content of calcite, and increasing microstructural surface area. Like prior studies on biogenic carbonates, this study utilized crushed shells in order to make their results relevant to sedimentary porewater systems and buffering of the seawater carbonate system. Modification of shell geometry and surface area through mechanical grinding, however, makes it challenging to apply their results to whole shell dissolution kinetics and the biological process of shell-building.

A handful of studies have investigated the dissolution kinetics of untreated, whole-shell biogenic carbonates. The earlier of these studies (Friedman, 1964; Schroeder, 1969; Land, 1967) focused mainly on the diagenetic stabilization of high-Mg calcite to form more stable low-Mg calcite and dolomite. As such, these experiments were carried out at temperatures and saturation states that are not relevant to conditions predicted for the future oceans. Moreover, rates of $CaCO_3$ dissolution in these experiments were typically not documented with the precision and accuracy needed for comparing results amongst organisms and/or experiments (Morse and Arvidson, 2002) or for interpreting these results in the context of future oceanic change.

More recent investigations of whole-shell dissolution kinetics (e.g., Morse et al., 1979; Keir, 1980; Bednaršek et al., 2012) were conducted with greater scientific rigor and over solution parameters more relevant to future oceanic change. However, these studies have largely been focused on planktonic calcifiers (e.g., foraminifera, coccolithophores, pteropods) due to their role in shelf, slope and deep-sea sedimentation.

Kennish and Lutz (1999) and Powell et al. (2008) conducted long-term field-based experiments and Glover and Kidwell (1993) conducted controlled laboratory experiments investigating the dissolution kinetics of bivalve shells, mainly from a taphonomic perspective (i.e., to determine the potential for preserving bivalve shells in the fossil record). And in a controlled laboratory experiment investigating dissolution rates of whole oyster shells over the pH range 7.2–7.9, Waldbusser et al. (2011) found that oyster shell dissolution rates increased with decreasing seawater pH, except between pH 7.4 and 7.2, and that fresh shells dissolved faster than weathered shells, which in turn dissolved faster than dredged shells.

Finally, Nash et al. (2013) conducted short-term (10-day) laboratory experiments investigating the dissolution rates of crustose coralline algae over the pH range 7.7–8.3 and found that algal skeletons rich in the less soluble dolomite mineral exhibited slower rates of dissolution than algal skeletons rich in the more-soluble Mg-calcite mineral.

Here, we seek to build upon this foundation of research investigating carbonate dissolution kinetics by conducting the first systematic analysis of whole-shell dissolution kinetics at various saturation states and temperatures for a range of benthic calcifying taxa spanning various polymorph mineralogies (aragonite, low-Mg calcite, high-Mg calcite).

2. MATERIALS AND METHODS

2.1. Specimen collection

Live organisms were collected, pursuant to local, state, and federal regulations, from the following localities: *M. edulis* (blue mussel) and *C. virginica* (oyster) from Buzzards Bay, Massachusetts; *B. eburneus* (ivory barnacle), *S. errata* (branching bryozoan), and *S. alatus* (conch) from the Gulf of Mexico off the coast of Florida; *Neogoniolithon* sp. (red alga) from the Atlantic Ocean off the coast of Florida; *M. mercenaria* (hard clam) and *M. arenaria* (soft clam) from Nantucket Sound off the coast of Massachusetts; *O. arbuscula* (temperate coral) from the Atlantic Ocean off the coast of North Carolina; and *S. siderea* (tropical coral) from the western Caribbean Sea off the coast of southern Belize. Prior to the start of the experiment, specimens were euthanized in 95% ethanol, gently cleaned of living tissue, rinsed in 95% ethanol to remove salts, and air-dried for 14 days. A small amount of cyanoacrylate epoxy (3–4 droplets) was used to re-attach left and right bivalve shells (clams, mussels, oysters) in order to mimic their articulated postures while alive. Initial dry weights were then obtained with a *Cole Parmer Symmetry PR 410* analytical balance.

2.2. Experimental conditions

Eighteen specimens of each species were submerged for 47 days in six sets of three-way replicated experimental pCO_2/temperature (±SD) treatments: (1) 497 ± 79 µatm/10.1 ± 0.2 °C; (2) 4144 ± 1194 µatm/10.1 ± 0.1 °C; (3) 5841 ± 1323 µatm/10.0 ± 0.2 °C; (4) 535 ± 76 µatm/24.9 ± 0.2 °C; (5) 4870 ± 1045 µatm/24.9 ± 0.2 °C; and (6) 9212 ± 1839 µatm/25.0 ± 0.2 °C (Table 1). The control pCO_2 gases were compressed air sourced from outside the building. The elevated pCO_2 gas mixtures were formulated by mixing pure compressed CO_2 with compressed air using *Aalborg* digital solenoid-valve mass flow controllers. The 34 L experimental tanks were formulated at salinity (±SD) of 32.0 (±0.1) with *Instant Ocean Sea Salt* mixed with deionized water and sterilized with addition of $HgCl_2$ (400 µL of saturated $HgCl_2$ solution per L seawater). Although the trace elemental composition of *Instant Ocean Sea Salt* differs subtly from that of natural seawater, its major and minor elemental composition, as well as its carbonate chemistry, was found to be the most similar to that of natural seawater when compared with eight other commercial sea salt mixes (Atkinson and Bingman, 1996). Seawater within each aquarium was continuously filtered (757 L h^{-1}) with a hanging power filter that contained a nylon-floss activated-carbon filter cartridge. Circulation and turbulence of seawater within aquaria were maintained with a 400 L h^{-1} powerhead in order to mimic flow conditions on the seafloor, as prior studies (e.g., Comeau et al., 2014) have shown that flow rates impact net calcification rates of benthic organisms. No illumination was provided to the aquaria. Each aquarium was covered with a transparent 3-mm thick plexiglass sheet and both the aquarium and the attached filtration system were wrapped with cellophane to promote equilibration between the gas mixtures and the experimental seawaters and to minimize evaporative water loss. Seawater temperatures (±SD) were maintained at the 25 °C target temperature with 50 watt heaters and at the 10 °C target temperature with 1 hp aquarium chillers. Each week, 250 mL seawater samples were obtained in ground-glass stoppered borosilicate glass bottles for the analysis of dissolved inorganic carbon (DIC) and total alkalinity (TA). Seventy-five percent seawater changes were performed weekly. Deionized water was also periodically added to the experimental aquaria in order to replenish water lost through evaporation and maintain the target salinity of 32.

2.3. Measurement and calculation of carbonate system parameters

Temperature within the experimental aquaria was measured every other day (Table 1) with a NIST-calibrated partial-immersion organic-filled glass thermometer. Salinity was measured every other day (Table 1) with a *YSI 3200* conductivity meter with a *YSI 3440* cell ($K = 10$) that was calibrated with seawater standards of known salinity provided by the laboratory of Prof. A. Dickson of Scripps Institute of Oceanography. Seawater dissolved inorganic carbon (DIC; Table 1) was measured via coulometry (*UIC 5400*) and total alkalinity (TA; Table 1) was measured via closed-cell potentiometric Gran titration.

Seawater pCO_2, pH, carbonate ion concentration ($[CO_3^{2-}]$), bicarbonate ion concentration ($[HCO_3^-]$), aqueous CO_2, and aragonite saturation state (Ω_A) were calculated with the program *CO2SYS* (Lewis and Wallace, 1998), using Roy et al. (1993) values for the K_1 and K_2 carbonic acid constants, the Mucci (1983) value for the stoichiometric aragonite solubility product, and an atmospheric pressure of 1.015 atm (Table 1).

2.4. Determination of whole-shell dissolution rates

Whole-shell dissolution rates were determined from the difference in whole-shell dry-weight between the beginning and end of the 47-day experiment. At the completion of the experiment, specimens were rinsed in 95% ethanol to remove salts and air-dried for 14 days. Dry weights of the specimens were obtained with a *Cole Parmer Symmetry PR 410* analytical balance. Gross dissolution rates were calculated as the percent change in dry-weight (change in dry weight divided by initial dry weight) in order to correct dissolution rates for initial shell surface area (proportional to mass), and normalized to the duration of the experiment (in days).

2.5. Modeling dissolution as a function of aragonite saturation state and temperature

Maximum likelihood non-linear hierarchical mixed effects modeling was employed to develop species-specific algorithms that predict shell dissolution rate as a function of aragonite saturation state and temperature (Tables 2 and 3). The general form of the model is an exponential asymptotic function that appeals to the general Arrhenius-derived rate equation for mineral dissolution [$r = (C \cdot e^{-E_a/RT})(1 - \Omega)^n$; terms defined above]:

$$y = B_0 - B_2 \cdot e^{B_1 \cdot \Omega}$$

where y = dissolution rate, B_0 = asymptote, B_1 = rate of approaching asymptote, B_2 = y-intercept and Ω = saturation state of seawater (cf. Morse and Arvidson, 2002; Gledhill and Morse, 2004, 2006a,b). Akaike's Information Criterion (AIC) was used to investigate various forms of B_0 and B_1, including treatment of each species and temperature combination as a structural unit [degrees of freedom (DF) = 8; AIC = −691.6], treatment of each species as a structural unit with temperature affecting only B_1 (DF = 8; AIC = −697.4), and treatment of each species as a structural unit with temperature affecting both B_1 and B_0 (DF = 9; AIC = −703.6). Since treatment of each species as a structural unit with temperature affecting both B_1 and B_0 yielded the lowest AIC, B_1 and B_0 were modeled as:

$$B_1 = b_1.\text{int} + b_1.\text{temp} + u_1,$$

$$B_0 = b_0.\text{int} + b_0.\text{temp} + u_0,$$

where b_0.int and b_1.int represent the fixed effects of aragonite saturation state, b_0.temp and b_1.temp represent the fixed effects of temperature, and u_0 and u_1 represent species-specific random effects. Thus, the maximum

Table 1
Average calculated [pCO_2 of gas in equilibrium with seawater ($pCO_{2\ (gas\text{-}e)}$), pH (seawater scale, pH_{SW}), carbonate ion concentration ($[CO_3^{2-}]$), bicarbonate ion concentration ($[HCO_3^-]$), dissolved CO_2 ($[CO_2]_{(SW)}$), and aragonite saturation state (Ω_A)] and measured [salinity (Sal), temperature (T), total alkalinity (TA), and dissolved inorganic carbon (DIC)] seawater parameters. SD = standard deviation; N = number of observations.

		497 µatm/ 10.1 °C	535 µatm/ 24.9 °C	4144 µatm/ 10.1 °C	4870 µatm/ 24.9 °C	5841 µatm/ 10.0 °C	9212 µatm/ 25.0 °C
Calculated parameters							
$pCO_{2\ (gas\text{-}e)}$	(µatm)	497	535	4144	4870	5841	9212
	SD	79	76	1194	1045	1323	1839
	Range	386–632	417–701	2111–5730	3598–7723	2395–7497	5323–12,433
	N	20	21	20	21	21	20
pH_{SW}		8.08	8.03	7.26	7.19	7.12	6.96
	SD	0.06	0.05	0.14	0.09	0.12	0.10
	Range	7.98–8.18	7.94–8.12	7.09–7.55	6.98–7.31	6.98–7.48	6.83–7.18
	N	20	21	20	21	21	20
$[CO_3^{2-}]$	(µM)	198	284	37	54	27	36
	SD	24	24	15	12	10	9
	Range	156–241	244–317	22–71	31–73	18–59	24–56
	N	20	21	20	21	21	20
$[HCO_3^-]$	(µM)	2629	2297	3154	2980	3261	3315
	SD	97	72	125	94	158	260
	Range	2488–2795	2172–2448	2920–3304	2813–3148	3064–3486	2917–3706
	N	20	21	20	21	21	20
$[CO_2]_{(SW)}$	(µM)	22	15	184	141	260	264
	SD	4	2	53	30	59	52
	Range	17–28	12–20	94–254	103–223	106–333	153–357
	N	20	21	20	21	21	20
Ω_A		3.0	4.6	0.6	0.9	0.4	0.6
	SD	0.4	0.4	0.2	0.2	0.1	0.2
	Range	2.4–3.7	3.9–5.1	0.3–1.1	0.5–1.2	0.3–0.9	0.4–0.9
	N	20	21	20	21	21	20
Measured parameters							
Sal	(psu)	32.03	32.07	31.96	32.02	32.01	32.06
	SD	0.10	0.10	0.09	0.22	0.08	0.12
	Range	31.80–32.20	31.90–32.30	31.80–32.20	31.50–32.30	31.90–32.20	31.80–32.30
	N	48	48	48	48	48	48
T	(°C)	10.1	24.9	10.1	24.9	10.0	25.0
	SD	0.2	0.2	0.1	0.2	0.2	0.2
	Range	9.7–10.6	24.3–25.2	9.9–10.6	24.2–25.2	9.7–10.5	24.8–26.1
	N	48	48	48	48	48	48
TA	(µM)	3087	2951	3235	3103	3317	3432
	SD	92	45	140	109	161	285
	Range	2983–3287	2897–3018	2972–3451	2899–3292	3116–3547	2982–3931
	N	21	21	21	21	21	21
DIC	(µM)	2847	2595	3381	3175	3520	3625
	SD	92	58	130	95	187	293
	Range	2723–3015	2501–2713	3180–3585	3024–3365	3140–3825	3190–4030
	N	21	21	21	21	21	21

likelihood non-linear mixed effects model of dissolution rate (y) as a function of aragonite saturation state (Ω_A) and temperature is:

$$y = (b_0.\text{int} + b_0.\text{temp} + u_0) - B_2 \cdot e^{(b_1.\text{int} + b_1.\text{temp} + u_1)\cdot\Omega_A}.$$

Fixed effects (b_1.int, b_1.temp, b_0.int, b_0.temp) were defined via normalized least squares regression analysis. Species-specific random effects parameters (u_0, u_1) were predicted via Log-Cholesky parameterization.

Although the shells and skeletons of the ten species investigated were composed of a range of calcium carbonate polymorphs (low-Mg calcite, high-Mg calcite, aragonite) with different solubility products, dissolution rates of all specimens were plotted and modeled with respect to the aragonite saturation state of seawater. This facilitated direct comparison of the dissolution responses of the different species (i.e., under equivalent future pCO_2 scenarios) and avoided problems associated with bi-mineralic shells

Table 2
Summary of statistical parameters for species-specific non-linear mixed effects models of dissolution rate. (A) Fixed effects parameters of the general exponential asymptotic function ($y = B_0 – B_2 \cdot e^{B_1 \Omega_A}$) used to model dissolution rate (y) as a function of aragonite saturation state (Ω_A) and temperature (T). $B_0 = b_0.\text{int} + b_0.\text{temp} + u_0$; $B_1 = b_1.\text{int} + b_1.\text{temp} + u_1$; SE = standard error; DF = degrees of freedom. (B) Species-specific random effects parameters u_0 and u_1 with condensed equations used to model species-specific dissolution rate (y) as a function of aragonite saturation state (Ω_A) and temperature (T).

(A)

Parameter	Value	SE	DF	T-value	P-value
B_2	0.6379	0.1128	183	5.6575	0.0000
b_0.int	−0.0250	0.0088	183	−2.8284	0.0052
b_1.int	−5.0299	0.6305	183	−7.9777	0.0000
b_0.temp	$0.0012 \cdot T + 0.0119$	0.0063	183	−2.8167	0.0054
b_1.temp	$0.0816 \cdot T + 0.8155$	0.2035	183	6.0101	0.0000

(B)

Specimen	Scientific name	u_0	u_1	Final condensed equation
American oyster	*Crassostrea virginica*	0.0129	−1.5334	$y = 0.0015 – 0.0012 \cdot T – 0.6379 \cdot e^{(-6.6214 \cdot \Omega_A + 0.0816 \cdot T \cdot \Omega_A)}$
Ivory barnacle	*Balanus eburneus*	0.0300	−1.8032	$y = -0.0002 – 0.0012 \cdot T – 0.6379 \cdot e^{(-7.3788 \cdot \Omega_A + 0.0816 \cdot T \cdot \Omega_A)}$
Blue mussel	*Mytilus edulis*	−0.0302	0.2137	$y = 0.0169 – 0.0012 \cdot T – 0.6379 \cdot e^{(-7.6486 \cdot \Omega_A + 0.0816 \cdot T \cdot \Omega_A)}$
Conch	*Strombus alatus*	−0.0162	2.4637	$y = 0.0050 – 0.0012 \cdot T – 0.6379 \cdot e^{(-6.7489 \cdot \Omega_A + 0.0816 \cdot T \cdot \Omega_A)}$
Tropical coral	*Siderastrea siderea*	0.0181	−0.9035	$y = -0.0255 – 0.0012 \cdot T – 0.6379 \cdot e^{(-6.1874 \cdot \Omega_A + 0.0816 \cdot T \cdot x)}$
Temperate coral	*Oculina arbuscula*	0.0209	−1.1125	$y = -0.0434 – 0.0012 \cdot T – 0.6379 \cdot e^{(-5.6317 \cdot \Omega_A + 0.0816 \cdot T \cdot \Omega_A)}$
Hard clam	*Mercenaria mercenaria*	0.0147	−0.7760	$y = 0.0078 – 0.0012 \cdot T – 0.6379 \cdot e^{(-6.9580 \cdot \Omega_A + 0.0816 \cdot T \cdot \Omega_A)}$
Soft clam	*Mya arenaria*	0.0049	2.1016	$y = 0.0045 – 0.0012 \cdot T – 0.6379 \cdot e^{(-4.5811 \cdot \Omega_A + 0.0816 \cdot T \cdot \Omega_A)}$
Branching bryozoan	*Schizoporella errata*	0.0176	1.2643	$y = -0.0293 – 0.0012 \cdot T – 0.6379 \cdot e^{(-3.3817 \cdot \Omega_A + 0.0816 \cdot T \cdot \Omega_A)}$
Coralline red alga	*Neogoniolithon* sp.	−0.0124	−0.3420	$y = -0.0082 – 0.0012 \cdot T – 0.6379 \cdot e^{(-3.7439 \cdot \Omega_A + 0.0816 \cdot T \cdot \Omega_A)}$

Table 3
Species-specific best-fit regressions used to model gross dissolution rate (y) as a function of aragonite saturation state (Ω_A) at 10.1 °C (±0.02) and 25.0 °C (±0.02).

Specimen	Scientific name	Temperature (°C)	Gross dissolution regression
American oyster	*Crassostrea virginica*	10	$y = -0.010 – 0.638 \cdot e^{(-6.621 \cdot \Omega_A + 0.816 \cdot \Omega_A)}$
		25	$y = -0.028 – 0.638 \cdot e^{(-6.621 \cdot \Omega_A + 2.039 \cdot \Omega_A)}$
Ivory barnacle	*Balanus eburneus*	10	$y = -0.012 – 0.638 \cdot e^{(-7.379 \cdot \Omega_A + 0.816 \cdot \Omega_A)}$
		25	$y = -0.030 – 0.638 \cdot e^{(-7.379 \cdot \Omega_A + 2.039 \cdot \Omega_A)}$
Blue mussel	*Mytilus edulis*	10	$y = 0.005 – 0.638 \cdot e^{(-7.649 \cdot \Omega_A + 0.816 \cdot \Omega_A)}$
		25	$y = -0.013 – 0.638 \cdot e^{(-7.649 \cdot \Omega_A + 2.039 \cdot \Omega_A)}$
Conch	*Strombus alatus*	10	$y = -0.007 – 0.638 \cdot e^{(-6.749 \cdot \Omega_A + 0.816 \cdot \Omega_A)}$
		25	$y = -0.025 – 0.638 \cdot e^{(-6.749 \cdot \Omega_A + 2.039 \cdot \Omega_A)}$
Tropical coral	*Siderastrea siderea*	10	$y = -0.037 – 0.638 \cdot e^{(-6.187 \cdot \Omega_A + 0.816 \cdot \Omega_A)}$
		25	$y = -0.055 – 0.638 \cdot e^{(-6.187 \cdot \Omega_A + 2.039 \cdot \Omega_A)}$
Temperate coral	*Oculina arbuscula*	10	$y = -0.055 – 0.638 \cdot e^{(-5.632 \cdot \Omega_A + 0.816 \cdot \Omega_A)}$
		25	$y = -0.073 – 0.638 \cdot e^{(-5.632 \cdot \Omega_A + 2.039 \cdot \Omega_A)}$
Hard clam	*Mercenaria mercenaria*	10	$y = -0.004 – 0.638 \cdot e^{(-6.958 \cdot \Omega_A + 0.816 \cdot \Omega_A)}$
		25	$y = -0.022 – 0.638 \cdot e^{(-6.958 \cdot \Omega_A + 2.039 \cdot \Omega_A)}$
Soft clam	*Mya arenaria*	10	$y = -0.007 – 0.638 \cdot e^{(-4.581 \cdot \Omega_A + 0.816 \cdot \Omega_A)}$
		25	$y = -0.025 – 0.638 \cdot e^{(-4.581 \cdot \Omega_A + 2.039 \cdot \Omega_A)}$
Branching bryozoan	*Schizoporella errata*	10	$y = -0.041 – 0.638 \cdot e^{(-3.382 \cdot \Omega_A + 0.816 \cdot \Omega_A)}$
		25	$y = -0.059 – 0.638 \cdot e^{(-3.382 \cdot \Omega_A + 2.039 \cdot \Omega_A)}$
Coralline red alga	*Neogoniolithon* sp.	10	$y = -0.020 – 0.638 \cdot e^{(-3.744 \cdot \Omega_A + 0.816 \cdot \Omega_A)}$
		25	$y = -0.038 – 0.638 \cdot e^{(-3.744 \cdot \Omega_A + 2.039 \cdot \Omega_A)}$

and with assigning solubility products to Mg-calcites of undetermined solubilities (see Pickett and Andersson, 2015). Should the reader prefer, the y-axes of the dissolution curves can be easily transformed to the appropriate polymorph since saturation states of calcium carbonate polymorphs are related by constant proportions. This

transformation would only expand or compress the dissolution curve along its x-axis; it would not materially alter the shape of the curve.

2.6. Estimation of gross calcification rates

Net calcification rates under a range of pCO_2 treatments at 25 °C have been previously determined for eight of the investigated organisms (Ries et al., 2009; Castillo et al., 2014). These measurements of net calcification represent the balance of gross calcification at the site of calcification and gross dissolution of previously formed shell/skeleton (Rodolfo-Metalpa et al., 2011). Gross calcification rates for eight of the investigated taxa were estimated by subtracting their empirically derived gross dissolution rates (this study) from their empirically derived net calcification rates derived by Ries et al. (2009; all taxa except *S. siderea*) and Castillo et al. (2014; *S. siderea* only) at the aragonite saturation states employed in the Ries et al. (2009) and Castillo et al. (2014) studies (Table 4). Although aragonite

Table 4
Estimated gross dissolution rates (this study), previously derived net calcification rates (Ries et al., 2009 – all species except *S. siderea*; Castillo et al., 2014 – *S. siderea*), and estimated gross calcification rates (net calcification minus gross dissolution) for eight species of marine calcifiers at 25.0 °C (±0.02) at Ω_A employed by Ries et al. (2009) and Castillo et al. (2014).

Specimen	Scientific name	Saturation state	Gross dissolution regression	Gross dissolution (%-wt per day)	Net calcification rate (%-wt per day)	Calculated gross calcification (%-wt per day)
American oyster	*Crassostrea virginica*	2.63	$y = -0.028 - 0.638 \cdot e^{(-6.621 \cdot \Omega_A + 2.039 \cdot \Omega_A)}$	−0.02817	0.03167	0.05983
		2.11		−0.02820	0.02667	0.05487
		1.43		−0.02907	0.01833	0.04740
		0.71		−0.05281	0.00500	0.05781
Blue mussel	*Mytilus edulis*	2.63	$y = -0.013 - 0.638 \cdot e^{(-7.649 \cdot \Omega_A + 2.039 \cdot \Omega_A)}$	−0.01279	0.07333	0.08612
		2.11		−0.01280	0.05167	0.06446
		1.43		−0.01300	0.06000	0.07300
		0.71		−0.02468	0.05167	0.07634
Conch	*Strombus alatus*	2.28	$y = -0.025 - 0.638 \cdot e^{(-6.749 \cdot \Omega_A + 2.039 \cdot \Omega_A)}$	−0.02473	0.03333	0.05806
		1.93		−0.02478	0.01333	0.03812
		1.51		−0.02523	0.02000	0.04523
		0.68		−0.05064	−0.05167	−0.00103
Tropical coral	*Siderastrea siderea*	3.97	$y = -0.055 - 0.638 \cdot e^{(-6.187 \cdot \Omega_A + 2.039 \cdot \Omega_A)}$	−0.05517	0.16500	0.22017
		2.83		−0.05517	0.22300	0.27817
		2.50		−0.05519	0.23600	0.29119
		1.06		−0.06289	0.15400	0.21689
Temperate coral	*Oculina arbuscula*	2.60	$y = -0.073 - 0.638 \cdot e^{(-5.632 \cdot \Omega_A + 2.039 \cdot \Omega_A)}$	−0.07308	0.19667	0.26975
		2.28		−0.07320	0.19333	0.26653
		1.64		−0.07479	0.18500	0.25979
		0.77		−0.11314	0.06333	0.17647
Hard clam	*Mercenaria mercenaria*	2.63	$y = -0.022 - 0.638 \cdot e^{(-6.958 \cdot \Omega_A + 2.039 \cdot \Omega_A)}$	−0.02190	0.01667	0.03857
		2.11		−0.02192	0.01167	0.03359
		1.43		−0.02246	0.00833	0.03079
		0.71		−0.04131	−0.02333	0.01797
Soft clam	*Mya arenaria*	2.63	$y = -0.025 - 0.638 \cdot e^{(-4.581 \cdot \Omega_A + 2.039 \cdot \Omega_A)}$	−0.02599	0.29167	0.31765
		2.11		−0.02818	0.12833	0.15651
		1.43		−0.04201	0.00333	0.04535
		0.71		−0.13011	−0.13500	−0.00489
Coralline red alga	*Neogoniolithon* sp.	3.12	$y = -0.038 - 0.638 \cdot e^{(-3.744 \cdot \Omega_A + 2.039 \cdot \Omega_A)}$	−0.04102	0.09500	0.13602
		2.40		−0.04855	0.24167	0.29021
		1.84		−0.06558	0.17833	0.24391
		0.90		−0.17540	0.06000	0.23540

saturation states employed in the dissolution experiment (this study) did not perfectly align with the aragonite saturation states employed in the prior studies from which net calcification rates were derived, non-linear mixed effects regressions were employed to interpolate gross dissolution rates at aragonite saturation states equivalent to those employed in the studies by Ries et al. (2009) and Castillo et al. (2014; Table 4). It should be noted that this approach to estimating gross calcification assumes that the gross dissolution of dead shell material is representative of the gross dissolution that would affect the shells of living organisms. Thus, values of gross calcification derived by subtracting measured gross dissolution from measured net calcification should be treated as estimates only. Indeed, the objective here is to identify general patterns of gross calcification amongst the organisms across a range of saturation states, rather than to generate highly accurate gross calcification rates for a given species at a given saturation state.

3. RESULTS

3.1. Effect of Ω_A on gross dissolution

All ten species of calcifiers exhibited gross dissolution curves that were asymptotic in nature. Dissolution rates were relatively constant in the treatments that were oversaturated with respect to organisms' predominant polymorph, and then predictably increased exponentially in the undersaturated treatments. Notably, gross dissolution of shells and skeletons of all investigated taxa were also observed in each of the oversaturated treatments ($\Omega_A > 1$) and at both temperatures (10, 25 °C), albeit at much slower rates than observed in the undersaturated treatments (Fig. 1).

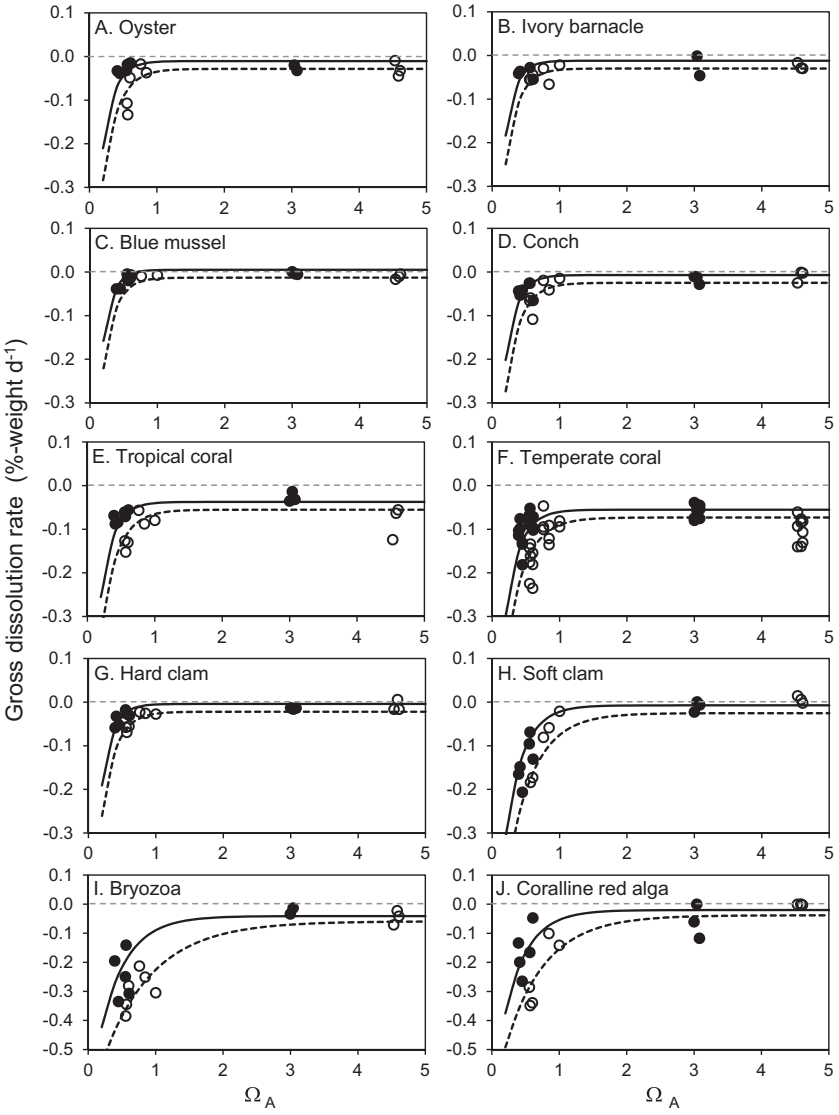

Fig. 1. Gross dissolution rate (%-weight per day) as a function of aragonite saturation state (Ω_A) at 10.1 °C (±0.02) (solid lines, closed circles) and 25.0 °C (±0.02) (dashed lines, open circles) for ten species of marine calcifiers. Horizontal dashed lines mark calcification-dissolution divide.

The asymptotic shape of the gross dissolution response curves allows them to be reliably modeled with an exponential asymptotic function ($y = B_0 – B_2 \cdot e^{B_1 \Omega}$; terms define above), which appeals to the general Arrhenius-derived rate equation for mineral dissolution [$r = (C \cdot e^{-E_a/RT})(1 - \Omega)^n$; terms defined above; cf. Gledhill and Morse, 2004, 2006a, 2006b; Morse and Arvidson, 2002].

Normalized least squares non-linear regression analysis was employed to define the following fixed effects of the dissolution rate model: b_0.int $= -0.0250$ ($p = 0.0052$); b_0.temp $= -0.0012 \cdot T + 0.0119$ ($p = 0.0054$); $b_2 = 0.6379$ ($p < 0.0001$); b_1.int $= -5.0299$ ($p = 0.0000$); and b_1.temp $= 0.0816 \cdot T - 0.8155$ ($p < 0.0001$; Table 2A). These statistically significant ($p < 0.01$) fixed effects parameters yield the following model of dissolution rate (y) as a function of aragonite saturation state (Ω_A) and temperature (T):

$$y = (-0.0250 + -0.0012 \cdot T + 0.0119 + u_0) - 0.6379 \cdot e^{(-5.0299 + 0.0816 \cdot T - 0.8155 + u_1) \cdot \Omega_A},$$

which can be condensed to:

$$y = -0.0131 – 0.0012 \cdot T + u_0 - 0.6379 \cdot e^{(-5.8454 + 0.0816 \cdot T + u_1) \cdot \Omega_A}.$$

Species-specific random effects parameters (u_0, u_1) were predicted via Log-Cholesky parameterization (Table 2B), resulting in species-specific models of shell dissolution from $\Omega_A = 0.2$ to $\Omega_A = 5.0$ as a function of aragonite saturation state and temperature (Fig. 1).

3.2. Effect of polymorph mineralogy on gross dissolution

Relative dissolution rates of the various shells and skeletons tracked the relative solubility of their predominant $CaCO_3$ polymorph: high-Mg calcite ≥ aragonite > low-Mg calcite (Table 5; Fig. 2). Largely high-Mg calcite shells [i.e., branching bryozoan (cf. Taylor et al., 2009; Smith, 2014) and coralline red algae] exhibited faster dissolution than predominantly aragonite shells (i.e., conch, tropical coral, temperate coral, hard clam and soft clam), which in turn experienced greater dissolution than predominantly low-Mg calcite shells (i.e., oyster, barnacle, mussel; see Ries (2011b) for mineralogical assays of the various species). However, dissolution rates did not track relative Mg-content of the two high-Mg calcite shells—the bryozoa (ca. 6 mol-% Mg; cf. Taylor et al., 2009; Smith, 2014) had higher dissolution rates than the more Mg-rich coralline red algae (>20 mol-% Mg; Ries, 2011b).

3.3. Effect of temperature on gross dissolution

Gross dissolution rates were modeled using the general equation $y = B_0 – B_2 \cdot e^{B_1 \Omega}$ and averaged at both 10.1 °C (±0.2) and 25.0 °C (±0.2) over $\Omega_A = 0.2$ to $\Omega_A = 5.0$. Dissolution rates at 10 °C were significantly ($p < 0.01$) lower than at 25 °C (Tables 2 and 5; Figs. 1 and 2). Shell/skeletal polymorph mineralogy impacted this effect of temperature on dissolution rate (Table 5; Fig. 2). Shells/skeletons composed predominantly of high-Mg calcite exhibited a stronger temperature-dissolution relationship than shells/skeletons composed largely of aragonite, which in turn exhibited a stronger temperature-dissolution relationship than shells/skeletons composed mostly of low-Mg calcite.

3.4. Estimated gross calcification in response to ocean acidification

Gross calcification rates under 25 °C for the oysters, blue mussels, conchs, tropical corals, temperate corals, hard clams, soft clams, and coralline red algae were estimated by subtracting gross dissolution rates (expressed as a negative value) at 25 °C in the present study from net calcification rates at 25 °C in the Ries et al. (2009) and Castillo et al. (2014) studies (Table 4; Fig. 3). These organisms' gross calcification response patterns to acidification were generally less severe (i.e., less steeply sloped) than their net calcification response patterns, as the latter incorporated the effects of gross dissolution of existing shell/skeleton. The two exceptions were the temperate and tropical corals, which exhibited similarly shaped but vertically offset gross calcifi-

Table 5
Effect of temperature and polymorph mineral solubility (high-Mg calcite ≥ aragonite > low-Mg calcite) on average modeled dissolution rate over $\Omega_A = 0.2$–5.0 (using Ω_A increments of 0.2) at 10.1 °C (±0.02) and 25.0 °C (±0.02). Results ranked by magnitude of temperature effect on average dissolution rate.

Specimen	Scientific name	Average dissolution rate (weight-% per day)			Mineralogy*
		10 °C	25 °C	Difference	
Blue mussel	*Mytilus edulis*	−0.0279	−0.0492	0.0213	LMC > A
Ivory barnacle	*Balanus eburneus*	−0.0456	−0.0673	0.0216	LMC
Hard clam	*Mercenaria mercenaria*	−0.0388	−0.0611	0.0223	A >> HMC
Conch	*Strombus alatus*	−0.0422	−0.0649	0.0227	A > LMC
American oyster	*Crassostrea virginica*	−0.0461	−0.0690	0.0230	LMC
Tropical coral	*Siderastrea siderea*	−0.0746	−0.0987	0.0241	A
Temperate coral	*Oculina arbuscula*	−0.0949	−0.1209	0.0260	A
Soft clam	*Mya arenaria*	−0.0538	−0.0867	0.0330	A >> HMC
Coralline red alga	*Neogoniolithon* sp.	−0.0754	−0.1228	0.0474	HMC
Branching bryozoan	*Schizoporella errata*	−0.1023	−0.1631	0.0608	HMC

* Polymorph mineralogy from Ries et al. (2009; all species except bryozoan and barnacle), Smith et al. (2006; bryozoan), and Bojar et al. (2012; barnacle); A – aragonite; LMC – low-Mg calcite (<4 mol% $MgCO_3$); HMC – high-Mg calcite (>4 mol% $MgCO_3$).

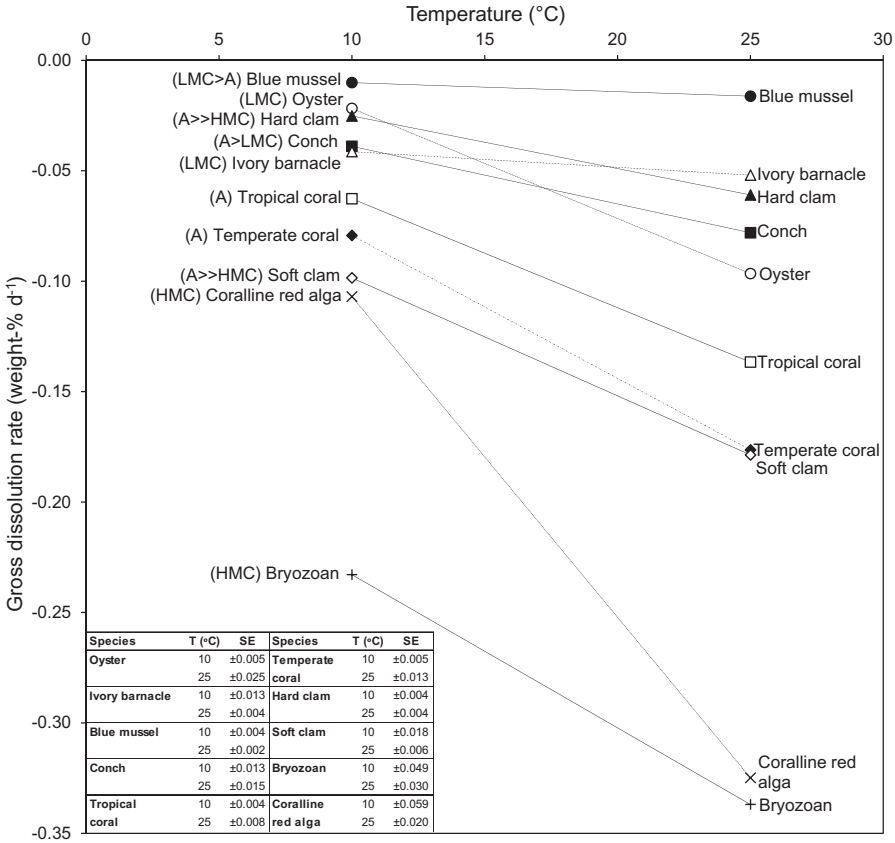

Species	T (°C)	SE	Species	T (°C)	SE
Oyster	10	±0.005	Temperate	10	±0.005
	25	±0.025	coral	25	±0.013
Ivory barnacle	10	±0.013	Hard clam	10	±0.004
	25	±0.004		25	±0.004
Blue mussel	10	±0.004	Soft clam	10	±0.018
	25	±0.002		25	±0.006
Conch	10	±0.013	Bryozoan	10	±0.049
	25	±0.015		25	±0.030
Tropical	10	±0.004	Coralline	10	±0.059
coral	25	±0.008	red alga	25	±0.020

Fig. 2. Effects of temperature (10, 25 °C) on rates of gross dissolution at $\Omega_A = 0.6$ for ten species of marine calcifiers. Rate of gross dissolution at 25 °C is higher than at 10 °C ($p < 0.05$) for all species. Magnitude of temperature effect on dissolution rate is generally proportional to polymorph solubility (high-Mg calcite ≥ aragonite > low-Mg calcite). Inset table shows standard errors (SE) of gross dissolution rates. 'A' – aragonite; 'LMC' – low-Mg calcite; 'HMC' – high-Mg calcite.

cation and net calcification response curves. Estimated gross calcification response patterns were most negative for the predominantly aragonite mollusks (conch, hard clam, soft clam), were flat for the predominantly calcite mollusks (oyster, mussel), were threshold in shape for the temperate coral (i.e., gross calcification declined drastically in the highest pCO_2 treatment), and parabolic in shape for the tropical coral and coralline red algae (i.e., gross calcification increased under moderately elevated pCO_2 but declined under the highest pCO_2 treatment).

4. DISCUSSION

4.1. Effect of Ω on gross dissolution rate

The observation that the gross dissolution curves for the investigated biogenic $CaCO_3$ exhibited trends similar to those of inorganic $CaCO_3$ and could be reasonably modeled with an exponential asymptotic function ($y = B_0 – B_2 \cdot e^{B_1 \Omega}$; terms define above) that appeals to the general Arrhenius-derived rate equation for mineral dissolution [$r = (C \cdot e^{-E_a/RT})(1 - \Omega)^n$; terms defined above; cf. Gledhill and Morse, 2004, 2006a, 2006b; Morse and Arvidson, 2002] suggests that the whole-shell dissolution kinetics of the investigated biogenic $CaCO_3$ generally conform to the dissolution kinetics of inorganic $CaCO_3$, as shown previously for shallow water marine carbonate sediments (e.g., Walter and Morse, 1985) and crushed biogenic carbonates (Pickett and Andersson, 2015).

However, the observation that gross dissolution of biogenic $CaCO_3$ occurred even in treatments that were oversaturated ($\Omega > 1$) with respect to both aragonite and calcite (albeit at much slower rates than in the undersaturated treatments) indicates that there are fundamental differences between the gross dissolution kinetics of biogenic and inorganic $CaCO_3$, with biogenic carbonates exhibiting greater vulnerability to dissolution than abiogenic carbonates, particularly at oversaturated conditions. These results contrast the work of Cubillas et al. (2005), which showed that biogenic carbonates dissolve more slowly than abiogenic carbonates of equivalent mineralogy when normalized to reactive (Brunauer-Emmett-Teller, BET) surface area, and at equivalent rates when normalized to geometric surface area.

The observed gross dissolution of biogenic $CaCO_3$ in oversaturated treatments could arise from various factors, including the dissolution of more soluble trace mineral phases, such as amorphous calcium carbonate (e.g. Weiner et al., 2003; Addadi et al., 2003), vaterite (Lowenstam and Abbott, 1975) or brucite (Schmalz, 1965), or from the disaggregation of organic matrices that

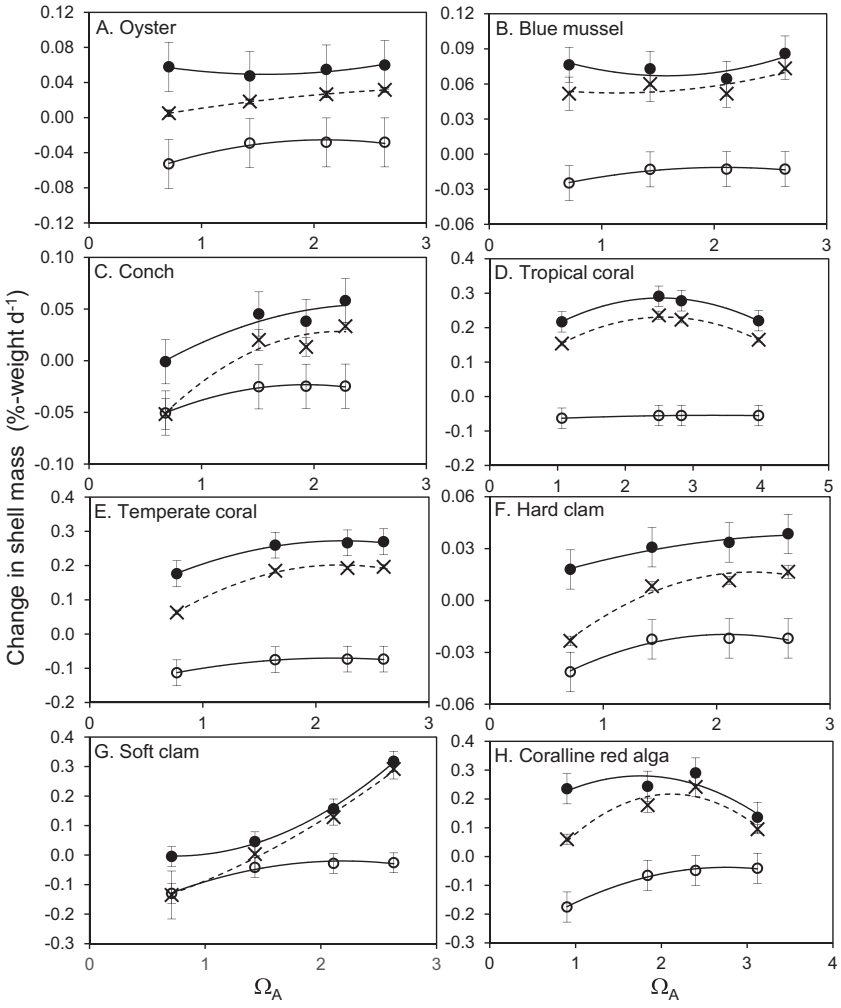

Fig. 3. Gross dissolution (open circle; estimated from this study), gross calcification (closed circle; net calcification minus gross dissolution), and net calcification ['*x*'; from Ries et al. (2009) and Castillo et al. (2014)] response curves [aragonite saturation state (Ω_A) vs. %-weight change per day] at 25.0 °C (±0.02) for eight species of marine calcifiers. Error bars represent standard error.

may bind together clusters and/or layers of biogenic carbonate minerals within shells and skeletons (e.g., Glover and Kidwell, 1993; Allemand et al., 1998). However, it is unlikely to have arisen from microbial-induced dissolution (e.g., Glover and Kidwell, 1993; Tribollet et al., 2009), as the experimental seawaters were poisoned with $HgCl_2$ for the duration of the experiment. Regardless of the precise mechanism that is responsible for the gross dissolution of biogenic carbonates in the oversaturated treatments, these results suggest that applying stoichiometric solubility products derived for inorganic carbonates to model gross dissolution of biogenic carbonates may substantially underestimate the impacts of ocean acidification on net calcification (gross calcification minus gross dissolution) of calcifying systems ranging in scale from individual organisms to entire ecosystems [as discussed in Andersson and Gledhill (2013) and Pickett and Andersson (2015) in the context of 'net ecosystem calcification'].

The observation that dissolution was observed within all of the investigated species, despite many of these species possessing some sort of organic covering on their outer surface (e.g., the periostraca for the 5 mollusk species investigated), indicates that such organic coverings do not, on their own, prevent shell dissolution.

4.2. Effect of $CaCO_3$ polymorph mineralogy on gross dissolution rate

Marine calcifiers build their shells from either the aragonite and/or calcite polymorphs of calcium carbonate, the latter of which can occur as either low-Mg (<4 mol-% Mg) or high-Mg (>4 mol-% Mg) phases. The aragonite polymorph is more soluble than the pure calcite phase. However, the solubility of calcite increases with increasing Mg-content, such that calcite with approximately 12 mol-% Mg has a solubility equivalent to that of aragonite. Shells and skeletons composed of aragonite and/or high-Mg calcite are therefore expected to be more deleteriously impacted by ocean acidification than those composed of low-Mg calcite (e.g., Andersson et al., 2007).

The present study reveals that gross dissolution rates at $\Omega_A = 0.6$ and $T = 10$ and 25 °C generally track shell/skele-

tal polymorph mineralogy (i.e., higher-Mg calcite ≥ aragonite > lower-Mg calcite; Table 5; Fig. 2). High-Mg calcite shells [i.e., branching bryozoa (cf. Taylor et al., 2009; Smith, 2014) and coralline red algae] exhibited more rapid dissolution than predominantly aragonite shells (i.e., conch, tropical coral, temperate coral, hard clam and soft clam), which in turn experienced faster dissolution than predominantly low-Mg calcite shells (i.e., oyster, barnacle and mussel). Notably, however, dissolution rates did not track relative Mg-content of the two high-Mg calcite shells—the bryozoan (ca. 6 mol-% Mg) had higher dissolution rates than the more Mg-rich coralline red algae (> 20 mol-% Mg). Pickett and Andersson (2015) also observed that crushed specimens of bryozoa had faster dissolution rates than crushed specimens of coralline red algae, despite the bryozoa's lower Mg-content. They attributed this trend to the bryozoan skeletons possessing proportionally more microstructural surface area than the coralline algae.

These results are consistent with the assertion that marine calcifiers that produce the more soluble phases of $CaCO_3$ (i.e., aragonite and high-Mg calcite) will be more vulnerable to the effects of ocean acidification than calcifiers that secrete less vulnerable phases (i.e., low-Mg calcite and dolomite; Andersson et al., 2008; Kuffner et al., 2008; Ries et al., 2009; Nash et al., 2013), although these trends can be moderated by differences in the microstructural surface area of the shells (Pickett and Andersson, 2015). These results are also consistent with the hypothesis that the average Mg-content of marine carbonate sediments may decrease with increasing ocean acidification due to the preferential dissolution of the more soluble higher-Mg phases (e.g., Morse et al., 2006; Andersson et al., 2008). This could ultimately lead to an oceanic state that favors the formation and preservation of low-Mg calcite shells and skeletons (historically known as 'calcite seas') over aragonite and high-Mg calcite shells and skeletons ('aragonite seas'; e.g., Mackenzie and Pigott, 1981; Sandberg, 1983; Andersson et al., 2006, 2008), despite that the relatively elevated Mg/Ca ratio of modern seawater (molar Mg/Ca = 5) kinetically favors the formation of aragonite and high-Mg calcite over low-Mg calcite ('aragonite seas'; cf. Ries, 2010).

4.3. Effect of temperature on dissolution rates

The results of the present study show that dissolution rates of all 10 species investigated were significantly ($p < 0.01$; Table 3) greater at a temperature of 25 °C than at a temperature of 10 °C (Tables 2 and 5; Figs. 1 and Fig. 2A). These results are consistent with the general equation for mineral dissolution rate that models the rate constant of the dissolution reaction with the Arrhenius equation [$r = (C \cdot e^{-E_a/RT})(1 - \Omega)^n$; see prior section for description of terms; cf. Gledhill and Morse, 2004, 2006a, 2006b; Morse and Arvidson, 2002], where increasing 'T' (temperature) results in increasing 'r' (surface-area-normalized dissolution rate). Temperature also has an indirect mitigating effect on dissolution rate because the solubility of CO_2 in seawater decreases with increasing temperature, resulting in increased Ω_A (cf. Andersson et al., 2008). Importantly, the results of the present study reveal that the increased rates of $CaCO_3$ dissolution that accompany a temperature increase from 10 to 25 °C outweigh any decrease in dissolution rate resulting from the temperature-induced increase in Ω_A (Fig. 1).

Furthermore, the magnitude of the temperature effect (10−25 °C) on dissolution rate was linked to shell/skeletal polymorph mineralogy (Table 5; Fig. 2). The effect of temperature on dissolution rates (quantified as the difference in average dissolution rate at 10 and 25 °C) was generally greater for high-Mg calcite shells/skeletons than for aragonite shells/skeletons, which were in turn generally greater than for low-Mg calcite shells/skeletons (Fig. 2). These results suggest that both ocean acidification and warming will disproportionately impact dissolution rates of shells and skeletons composed of the more soluble phases of calcium carbonate (i.e., higher-Mg calcite and aragonite).

4.4. Surface area effects

Calcifying organisms utilize a broad range of microstructures in the construction of their shells and skeletons. Carriker et al. (1991), for example, documented 4 discrete microstructural groups within a single oyster shell, each with potentially unique dissolution kinetics. Walter and Morse (1985) also showed that relative dissolution rates of carbonate sediments were impacted by their reactive surface area. And Kidwell (2001) argued that shell microstructure is a key factor in determining whether a species is ultimately preserved in the fossil record, or lost to dissolution. It is therefore likely that both shell microstructure and macro-structure played a role in determining relative dissolution rates of the different shell types investigated in the present study. For instance, the 6 mol-% Mg calcite skeletons of the bryozoa dissolved more rapidly than the more soluble >20 mol-% calcite skeletons of the coralline red algae. Pickett and Andersson (2015) recently attributed a similar trend that they observed for crushed samples of bryozoa and coralline red algae to the bryozoan skeleton having a higher surface-area-to-volume-ratio than the skeleton of the coralline red algae. However, the irregular geometry and relatively large size of the shells investigated in the present study precluded analysis of their reactive surface areas via traditional methods, such as morphometric analysis and BET gas adsorption. Instead, geometric effects were controlled for by normalizing shell dissolution rates to starting shell mass, which should generally be proportional to surface area.

4.5. Gross calcification responses to elevated pCO_2

Estimation of gross calcification rates (Table 4; Fig. 3) from empirically derived rates of net calcification (Ries et al., 2009; Castillo et al., 2014) and gross dissolution (this study) reveals that all eight taxa, including the conch, hard clam, and coralline red algae that exhibited net dissolution under the highest pCO_2 treatment, were able to continue calcifying on a gross basis in all four pCO_2 treatments—including the treatment undersaturated with respect to aragonite. Notably, the organisms' gross calcification response patterns to acidification were generally less severe

(i.e., less steeply sloped) than their net calcification response patterns. This suggests that the shape of an organism's net calcification response pattern to ocean acidification—particularly in conditions approaching or exceeding undersaturation with respect to their mineral polymorph—is largely influenced by the gross dissolution of their shell or skeleton, rather than simply by their gross calcification under those conditions.

The observation that gross calcification response patterns were most negative for the predominantly aragonite mollusks (conch, hard clam, soft clam), were flat for the predominantly calcite mollusks (oyster, mussel), were threshold in shape for the temperate coral, and parabolic in shape for the tropical coral and coralline red algae (Table 4; Fig. 3), is consistent with prior observations that marine calcifiers exhibit highly variable calcification responses to CO_2-induced ocean acidification (Ries et al., 2009; Kroeker et al., 2010; Hendricks et al., 2010).

Ries et al. (2009) attributed these differential responses to a confluence of factors, including the relative solubility of their mineral polymorph, the extent to which they utilize organic coverings (e.g., epicuticles in crustacea, periostraca in mollusks, calicoblastic epithelia in corals) to protect their shells or skeletons from external seawater, the extent to which they utilize CO_2 directly via photosynthesis, and their relative ability to remove protons from their calcifying fluid in order to deprotonate HCO_3^- to generate CO_3^{2-} for calcification (see Jokiel, 2011; Ries, 2011c; Bach, 2015, for further discussion). The observation that the aragonite mollusks exhibited a more negative response than the calcite mollusks (Fig. 3) is consistent with the assertion that shell polymorph mineralogy plays a role in determining differential gross calcification responses to ocean acidification *within* taxonomic classes. However, the observation that the high-Mg calcite coralline red algae, which produce a highly soluble polymorph of $CaCO_3$, exhibited the most positive gross calcification response to acidification (Fig. 3) suggests that polymorph mineral solubility is not the primary factor controlling polyphyletic trends in gross calcification responses to ocean acidification.

The observation that the mollusks, which are thought to maintain their calcifying fluid at pH similar to that of seawater (e.g., Crenshaw, 1972), generally exhibited a more negative gross calcification response to acidification than the corals and algae, which are thought to maintain their calcifying fluids at a substantially elevated pH (Al-Horani et al., 2003; Cohen et al., 2009; Krief et al., 2010; Trotter et al., 2011; Venn et al., 2011; Ries, 2011c; Anagnostou et al., 2012; McCulloch et al., 2012; Holcomb et al., 2014), is consistent with the assertion that organisms' ability to elevate pH at the site of calcification is an important factor in determining cross-taxonomic trends in gross calcification responses to ocean acidification (Ries et al., 2009).

Lastly, the observation that the photosynthesizing organisms that were investigated (corals and coralline algae) exhibited more positive gross calcification responses to CO_2-induced ocean acidification (i.e., parabolic in shape for the tropical corals and coralline algae) than the non-photosynthesizing organisms investigated (mollusks) suggests that an organisms' ability to utilize CO_2 directly via photosynthesis also influences cross-taxonomic trends in gross calcification responses to ocean acidification. In brief, moderate increases in pCO_2 may fertilize photosynthesis in some symbiont bearing corals and coralline algae, thereby providing additional energy for calcification and resulting in a positive calcification response to moderate ocean acidification (i.e., defining the up-slope of the parabola). Under extreme elevations in pCO_2, when aqueous CO_2 is no longer limiting for photosynthesis, the negative impacts of reduced $CaCO_3$ saturation state may outweigh the benefits of increased (or CO_2-saturated) photosynthesis, resulting in a negative calcification response to extreme ocean acidification (i.e., defining the down-slope of the parabola). More thorough discussions of the competing effects of CO_2-enhanced photosynthesis versus CO_2-impaired calcification in determining corals' calcification response to ocean acidification are available in Ries et al. (2009) and Castillo et al. (2014).

5. CONCLUSIONS

Whole-shell dissolution experiments conducted across a range of saturation states ($0.4 < \Omega_A < 4.6$) and temperatures (10, 25 °C) on ten species of marine calcifiers revealed the following:

(1) Dissolution rates of whole-shell biogenic carbonates decrease with $CaCO_3$ saturation state, increase with temperature, and vary predictably with respect to the relative solubility of the calcifiers' shell polymorph mineralogy [high-Mg calcite (mol% Mg > 4) ≥ aragonite > low-Mg calcite (mol% Mg < 4)], consistent with prior studies on sedimentary and inorganic carbonates. These results indicate that both ocean acidification *and* warming will increase dissolution rates of biogenic carbonates in future oceans.

(2) The severity of the temperature effects on gross dissolution rates varied with respect to carbonate polymorph solubility, with warming (10–25 °C) exerting the greatest effect on biogenic high-Mg calcite, an intermediate effect on biogenic aragonite, and the least effect on biogenic low-Mg calcite.

(3) Gross dissolution curves for the investigated biogenic $CaCO_3$ were similar in shape to those of inorganic $CaCO_3$ and could be reasonably modeled with an exponential asymptotic function ($y = B_0 - B_2 \cdot e^{B_1 \Omega}$) that appeals to the general Arrhenius-derived rate equation for mineral dissolution [$r = (C \cdot e^{-E_a/RT})(1 - \Omega)^n$].

(4) Gross dissolution of whole-shell biogenic $CaCO_3$ occurred even in treatments that were oversaturated ($\Omega > 1$) with respect to both aragonite and calcite, indicating that fundamental differences exist between the dissolution kinetics of whole-shell and inorganic $CaCO_3$. Therefore, applying stoichiometric solubility products derived for inorganic carbonates to model gross dissolution of biogenic carbonates may substantially underestimate the impacts of ocean acidification on net calcification (gross calcification minus

gross dissolution) of calcifying systems ranging in scale from individual organisms to entire ecosystems (i.e., net ecosystem calcification).

(5) Rough estimates of the impact of ocean acidification on the gross calcification rates of various species of marine calcifiers were calculated from the difference between rates of net calcification (determined in prior studies) and gross dissolution (determined in present study). Organisms' gross calcification responses to acidification were generally less severe than their net calcification response patterns, with aragonite mollusks (bivalves, gastropods) exhibiting the most negative gross calcification response to acidification, and photosynthesizing organisms (corals, coralline red algae) exhibiting greater resilience.

ACKNOWLEDGEMENTS

We thank K. Horvath and T. Courtney for valuable input and assistance. We thank C. Pelejero and an anonymous referee for their thorough reviews. This research was supported by NOAA awards NA13OAR4310186 (to JBR and KDC) and NA14NMF4540072 (to JBR), the UNC-Chapel Hill IDEA Program (NSF award #1107897, in support of MNG), and NSF awards OCE-1437371 and OCE-1459706 (to JBR). This is contribution number 340 of the Marine Science Center at Northeastern University.

REFERENCES

Addadi L., Raz S. and Weiner S. (2003) Taking advantage of disorder: amorphous calcium carbonate and its roles in biomineralization. *Adv. Mater.* **15**, 959–970.

Akin G. W. and Lagerwerff J. V. (1965) Calcium carbonate equilibrium in aqueous solutions open to the air: II. Enhanced solubility of a $CaCO_3$ in the presence of Mg^{2+} and SO_4^{2-}. *Geochim. Cosmochim. Acta* **29**, 353–360.

Al-Horani F. A., Al-Moghrabi S. M. and DeBeer D. (2003) The mechanism of calcification and its relation to photosynthesis and respiration in the scleractinian coral *Galaxea fascicularis*. *Mar. Biol.* **142**, 419–426.

Alkattan M., Oelkers E. H., Dandurand J.-L. and Schott J. (1998) An experimental study of calcite and limestone dissolution rates as a function of pH from −1 to 3 and temperature from 25 to 80 °C. *Chem. Geol.* **151**, 199–214.

Alkattan M., Oelkers E. H., Dandurand J.-L. and Schott J. (2002) An experimental study of calcite dissolution rates at acidic conditions and 25 °C in the presence of $NaPO_3$ and $MgCl_2$. *Chem. Geol.* **190**, 291–302.

Allemand D., Tambutté É., Girard J.-P. and Jaubert J. (1998) Organic matrix synthesis in the scleractinian coral *Stylophora pistillata*: role in biomineralization and potential target of the organotin tributyltin. *J. Exp. Biol.* **201**, 2001–2009.

Amrhein C., Jurinak J. J. and Moore W. M. (1985) Kinetics of calcite dissolution as affected by carbon dioxide partial pressure. *Soil Sci. Soc. Am. J.* **49**, 1393–1398.

Anagnostou E., Huang K. F., You C. F., Sikes E. L. and Sherrell R. M. (2012) Evaluation of boron isotope ratio as a pH proxy in the deep sea coral *Desmophyllum dianthus*: evidence of physiological pH adjustment. *Earth Planet. Sci. Lett.* **349–350**, 251–260.

Andersson A. J. and Gledhill D. (2013) Ocean acidification and coral reefs: effects on breakdown, dissolution, and net ecosystem calcification. *Annu. Rev. Mar. Sci.* **5**, 321–348.

Andersson A. J., Mackenzie F. T. and Gattuso J.-P. (2011) Effects of ocean acidification on benthic processes, organisms, and ecosystems in Ocean Acidification (eds. J.-P. Gattuso and L. Hansson). Oxford University Press, Oxford, England, pp. 112–153.

Andersson A. J. and Mackenzie F. T. (2012) Revisiting four scientific debates in ocean acidification research. *Biogeosciences* **9**, 893–905.

Andersson A. J., Mackenzie F. T. and Lerman A. (2005) Coastal ocean and carbonate systems in the high-CO_2 world of the Anthropocene. *Am. J. Sci.* **305**, 875–918.

Andersson A. J., Mackenzie F. T. and Lerman A. (2006) Coastal ocean CO_2–carbonic acid–carbonate sediment system of the Anthropocene. *Global Biogeochem. Cycles* **20**.

Andersson A. J., Bates N. R. and Mackenzie F. T. (2007) Dissolution of carbonate sediments under rising pCO_2 and ocean acidification: observations from Devil's Hole, Bermuda. *Aquat. Geochem.* **13**, 237–264.

Andersson A. J., Mackenzie F. T. and Bates N. R. (2008) Life on the margin: implications of ocean acidification on Mg-calcite, high latitude and cold-water marine calcifiers. *Mar. Ecol. Prog. Ser.* **373**, 265–273.

Andersson A. J., Kuffner I. B., Mackenzie F. T., Jokiel P., Rodgers K. S. and Tan A. (2009) Net loss of $CaCO_3$ from a subtropical calcifying community due to seawater acidification: mesocosm-scale experimental evidence. *Biogeosciences* **6**, 1811–1823.

Arakaki T. and Mucci A. (1995) A continuous and mechanistic representation of calcite reaction-controlled kinetics in dilute solutions at 25 C and 1 atm total pressure. *Aquat. Geochem.* **1**, 105–130.

Archer D., Emerson S. and Reimers C. (1989) Dissolution of calcite in deep-sea sediments: pH and O_2 microelectrode results. *Geochim. Cosmochim. Acta* **53**, 2831–2845.

Arvidson R. S. and Luttge A. (2010) Mineral dissolution kinetics as a function of distance from equilibrium – new experimental results. *Chem. Geol.* **269**, 79–88.

Arvidson R. S., Ertan I. E., Amonette J. E. and Luttge A. (2003) Variation in calcite dissolution rates: a fundamental problem? *Geochim. Cosmochim. Acta* **67**, 1623–1634.

Arvidson R. S., Collier M., Davis K. J., Vinson M. D., Amonette J. E. and Luttge A. (2006) Magnesium inhibition of calcite dissolution kinetics. *Geochim. Cosmochim. Acta* **70**, 583–594.

Atkinson M. and Bingman C. (1996) Elemental composition of commercial seasalts. *J. Aquaricult. Aquat. Sci.* **8**, 39–43.

Bach L. T. (2015) Reconsidering the role of carbonate ion concentration in calcification by marine organisms. *Biogeosciences* **12**, 4939–4951.

Balzer W. and Wefer G. (1981) Dissolution of carbonate minerals in a subtropical shallow marine environment. *Mar. Chem.* **10**, 545–558.

Barwise A. J., Compton R. G. and Unwin P. R. (1990) The effect of carboxylic acids on the dissolution of calcite in aqueous solution. Part 2. d-, l- and meso-Tartaric acids. *J. Chem. Soc. Faraday Trans.* **86**, 137–144.

Baumann J., Buhmann D., Dreybrodt W. and Schulz H. D. (1985) Calcite dissolution kinetics in porous media. *Chem. Geol.* **53**, 219–228.

Bednaršek N., Tarling G. A., Bakker D. C. E., Fielding S., Jones E. M., Venables H. J., Ward P., Kuzirian A., Leze B. and Feely R. A. (2012) Extensive dissolution of live pteropods in the Southern Ocean. *Nat. Geosci.* **5**, 881–885.

Berger W. H. (1967) Foraminiferal ooze: solution at depth. *Science* **156**, 383–385.

Berner R. A. (1967) Comparative dissolution characteristics of carbonate minerals in the presence and absence of aqueous magnesium ion. *Am. J. Sci.* **265**, 45–70.
Berner R. A. (1978) Rate control of mineral dissolution under earth surface conditions. *Am. J. Sci.* **278**, 1235–1252.
Berner R. A. and Morse J. W. (1974) Dissolution kinetics of calcium carbonate in sea water: IV. Theory of calcite dissolution. *Am. J. Sci.* **274**, 108–134.
Bertram M. A., Mackenzie F. T., Bishop F. C. and Bischoff W. D. (1991) Influence of temperature on the stability of magnesian calcite. *Am. Mineral.* **76**, 1889–1896.
Bischoff W. D. (1998) Dissolution enthalpies of magnesian calcites. *Aquat. Geochem.* **4**, 321–336.
Bischoff W. D., Bishop F. C. and Mackenzie F. T. (1983) Biogenically produced magnesian calcite: inhomogeneities in chemical and physical properties and comparison with synthetic phases. *Am. Mineral.* **68**, 1183–1188.
Bischoff W. D., Mackenzie F. T. and Bishop F. C. (1987) Stabilities of synthetic magnesian calcites in aqueous solution: comparison with biogenic materials. *Geochim. Cosmochim. Acta* **51**, 1413–1423.
Bojar A. V., Bojar H. P. and Tufar W. (2012) Mg/Ca and isotopic high resolution record of deep-sea hydrothermal barnacles. *EGU General Assembly Conference Abstracts* **14**, 12862.
Boucher G., Clavier J., Hily C. and Gattuso J. P. (1998) Contribution of soft-bottoms to the community metabolism (primary production and calcification) of a barrier reef flat (Moorea, French Polynesia). *J. Exp. Mar. Biol. Ecol.* **225**, 269–283.
Brewer P. G. (1997) Ocean chemistry of the fossil fuel CO_2 signal: the haline signal of "business as usual". *Geophys. Res. Lett.* **24**, 1367–1369.
Buhmann D. and Dreybrodt W. (1985a) The kinetics of calcite dissolution and precipitation in geologically relevant situations of karst areas: 1. Open system. *Chem. Geol.* **48**, 189–211.
Buhmann D. and Dreybrodt W. (1985b) The kinetics of calcite dissolution and precipitation in geologically relevant situations of karst areas: 2. Closed system. *Chem. Geol.* **53**, 109–124.
Buhmann D. and Dreybrodt W. (1987) Calcite dissolution kinetics in the system H_2O–CO_2–$CaCO_3$ with participation of foreign ions. *Chem. Geol.* **64**, 89–102.
Burdige D. J. and Zimmerman R. C. (2002) Impact of sea grass density on carbonate dissolution in Bahamian sediments. *Limnol. Oceanogr.* **47**, 1751–1763.
Burdige D. J., Zimmerman R. C. and Hu X. (2008) Rates of carbonate dissolution in permeable sediments estimated from pore-water profiles: the role of sea grasses. *Limnol. Oceanogr.* **53**, 549.
Burdige D. J., Hu X. and Zimmerman R. C. (2010) The widespread occurrence of coupled carbonate dissolution/reprecipitation in surface sediments on the Bahamas Bank. *Am. J. Sci.* **310**, 492–521.
Busenberg E. and Plummer L. N. (1986) A comparative study of the dissolution and crystal growth kinetics of calcite and aragonite. *Stud. Diagenesis* **105**, 139–168.
Caldeira K. and Wickett M. E. (2003) Oceanography: anthropogenic carbon and ocean pH. *Nature* **425**, 365–365.
Carriker M. R., Swann C. P., Prezant R. S. and Counts C. L. (1991) Chemical elements in the aragonitic and calcitic microstructural groups of shell of the oyster *Crassostrea virginica*: a proton probe study. *Mar. Biol.* **109**, 287–297.
Casey W. H. and Sposito G. (1992) On the temperature dependence of mineral dissolution rates. *Geochim. Cosmochim. Acta* **56**, 3825–3830.
Castillo K. D., Ries J. B., Bruno J. F. and Westfield I. T. (2014) The reef-building coral *Siderastrea siderea* exhibits parabolic responses to ocean acidification and warming. *Proc. R. Soc. B: Biol. Sci.* **281**, 20141856.
Chou L., Garrels R. M. and Wollast R. (1989) Comparative study of the kinetics and mechanisms of dissolution of carbonate minerals. *Chem. Geol.* **78**, 269–282.
Cohen S. and Fine M. (2012) Measuring gross and net calcification of a reef coral under ocean acidification conditions: methodological considerations. *Biogeosci. Discuss.* **9**, 8241–8272.
Cohen A., McCorkle D., de Putron S. A. G. G. and Rose K. A. (2009) Morphological and compositional changes in the skeletons of new coral recruits reared in acidified seawater: insights into the biomineralization response to ocean acidification. *Geochem. Geophys. Geosyst.* **10**, Q07005.
Comeau S., Gorsky G., Alliouane S. and Gattuso J.-P. (2010) Larvae of the pteropod *Cavolinia inflexa* exposed to aragonite under saturation are viable but shell-less. *Mar. Biol.* **157**, 2341–2345.
Comeau S., Edmunds P. J., Lantz C. A. and Carpenter R. C. (2014) Water flow modulates the response of coral reef communities to ocean acidification. *Sci. Rep.* **4**. http://dx.doi.org/10.1038/srep06681.
Compton R. G. and Pritchard K. L. (1990) The dissolution of calcite at pH < 7: kinetics and mechanism. *Philos. Trans. R. Soc. Lond.: Series A Math. Phys. Sci.* **330**, 47–70.
Compton R. G. and Sanders G. H. W. (1993) The dissolution of calcite in aqueous acid: the influence of humic species. *J. Colloid Interface Sci.* **158**, 439–445.
Compton R. G. and Unwin P. R. (1990) The dissolution of calcite in aqueous solution at pH < 4: kinetics and mechanism. *Philos. Trans. R. Soc. Lond.: Series A Math. Phys. Sci.*, 1–45.
Compton R. G., Daly P. J. and Houses W. A. (1986) The dissolution of Iceland spar crystals: the effect of surface morphology. *J. Colloid Interface Sci.* **113**, 12–20.
Compton R. G., Pritchard K. L. and Unwin P. R. (1989) The dissolution of calcite in acid waters: mass transport versus surface control. *Freshw. Biol.* **22**, 285–288.
Crenshaw M. A. (1972) The inorganic composition of molluscan extrapallial fluid. *Biol. Bull.* **143**, 506–512.
Cubillas P., Köhler S., Prieto M., Chaïrat C. and Oelkers E. H. (2005) Experimental determination of the dissolution rates of calcite, aragonite, and bivalves. *Chem. Geol.* **216**, 59–77.
Doney S. C., Fabry V. J., Feely R. A. and Kleypas J. A. (2009) Ocean acidification: the other CO_2 problem. *Mar. Sci.* **1**.
Donner S. D. (2009) Coping with commitment: projected thermal stress on coral reefs under different future scenarios. *PLoS ONE* **4**, e5712.
Dreybrodt W. (1981) Kinetics of the dissolution of calcite and its applications to karstification. *Chem. Geol.* **31**, 245–269.
Dreybrodt W. and Buhmann D. (1991) A mass transfer model for dissolution and precipitation of calcite from solutions in turbulent motion. *Chem. Geol.* **90**, 107–122.
Dreybrodt W., Lauckner J., Zaihua L., Svensson U. and Buhmann D. (1996) The kinetics of the reaction $CO_2 + H_2O \rightarrow H^+ + HCO_3^-$ as one of the rate limiting steps for the dissolution of calcite in the system H_2O–CO_2–$CaCO_3$. *Geochim. Cosmochim. Acta* **60**, 3375–3381.
Eakin C. M., Kleypas J. and Hoegh-Guldberg O. (2008) Global climate change and coral reefs: rising temperatures, acidification and the need for resilient reefs. In *Status of Coral Reefs of the World* (ed. C. Wilkinson), pp. 29–34.
Egleston E. S., Sabine C. L. and Morel F. M. (2010) Revelle revisited: buffer factors that quantify the response of ocean chemistry to changes in DIC and alkalinity. *Global Biogeochem. Cycles* **24**.
Eisenlohr L., Meteva K., Gabrovšek F. and Dreybrodt W. (1999) The inhibiting action of intrinsic impurities in natural calcium

carbonate minerals to their dissolution kinetics in aqueous H_2O–CO_2 solutions. *Geochim. Cosmochim. Acta* **63**, 989–1001.
Fabricius K. E., Langdon C., Uthicke S., Humphrey C., Noonan S., De'ath G., Okazaki R., Muehllehner N., Glas M. S. and Lough J. M. (2011) Losers and winners in coral reefs acclimatized to elevated carbon dioxide concentrations. *Nat. Clim. Change* **1**, 165–169.
Fabry V. J., Seibel B. A., Feely R. A. and Orr J. C. (2008) Impacts of ocean acidification on marine fauna and ecosystem processes. *ICES J. Mar. Sci.* **65**, 414–432.
Feely R. A., Sabine C. L., Hernandez-Ayon J. M., Ianson D. and Hales B. (2008) Evidence for upwelling of corrosive 'acidified' water onto the continental shelf. *Science* **320**, 1490–1492.
Finneran D. W. and Morse J. W. (2009) Calcite dissolution kinetics in saline waters. *Chem. Geol.* **268**, 137–146.
Friedman G. M. (1964) Early diagenesis and lithification in carbonate sediments. *J. Sediment. Res.* **34**.
Füssel H.-M. (2009) *Review and quantitative analysis of indices of climate change exposure, adaptive capacity, sensitivity, and impacts*. World Bank, Washington, DC.
Garrels R. M. and Wollast R. (1978) Equilibrium criteria for two-component solids reacting with fixed composition in an aqueous phase; example, the magnesian calcites; discussion. *Am. J. Sci.* **278**, 1469–1474.
Garrels R. M., Thompson M. E. and Siever R. (1960) Stability of some carbonates at 25 °C and one atmosphere total pressure. *Am. J. Sci.* **258**, 402–418.
Garrels R. M., Thompson M. E. and Siever R. (1961) Control of carbonate solubility by carbonate complexes. *Am. J. Sci.* **259**, 24–45.
Gehlen M., Bassinot F. C., Chou L. and McCorkle D. (2005a) Reassessing the dissolution of marine carbonates: I. Solubility. *Deep Sea Res. Part I* **52**, 1445–1460.
Gehlen M., Bassinot F. C., Chou L. and McCorkle D. (2005b) Reassessing the dissolution of marine carbonates: II. Reaction kinetics. *Deep Sea Res. Part I* **52**, 1461–1476.
Gledhill D. K. and Morse J. W. (2004) Dissolution kinetics of calcite in NaCl–$CaCl_2$–$MgCl_2$ brines at 25 °C and 1 bar pCO_2. *Aquat. Geochem.* **10**, 171–190.
Gledhill D. K. and Morse J. W. (2006a) Calcite dissolution kinetics in Na–Ca–Mg–Cl brines. *Geochim. Cosmochim. Acta* **70**, 5802–5813.
Gledhill D. K. and Morse J. W. (2006b) Calcite solubility in Na–Ca–Mg–Cl brines. *Chem. Geol.* **233**, 249–256.
Glover C. P. and Kidwell S. M. (1993) Influence of organic matrix on the post-mortem destruction of molluscan shells. *J. Geol.* **101**, 729–747.
Gutjahr A., Dabringhaus H. and Lacmann R. (1996) Studies of the growth and dissolution kinetics of the $CaCO_3$ polymorphs calcite and aragonite II. The influence of divalent cation additives on the growth and dissolution rates. *J. Cryst. Growth* **158**, 310–315.
Hales B. and Emerson S. (1996) Calcite dissolution in sediments of the Ontong-Java Plateau: in situ measurements of pore water O_2 and pH. *Global Biogeochem. Cycles* **10**, 527–541.
Hales B., Emerson S. and Archer D. (1994) Respiration and dissolution in the sediments of the western North Atlantic: estimates from models of in situ microelectrode measurements of porewater oxygen and pH. *Deep Sea Res. Part I* **41**, 695–719.
Harstad A. and Stipp S. L. S. (2007) Calcite dissolution: effects of trace cations naturally present in Iceland spar calcites. *Geochim. Cosmochim. Acta* **71**, 56–70.
He S. and Morse J. W. (1993) The carbonic acid system and calcite solubility in aqueous Na–K–Ca–Mg–Cl–SO_4 solutions from 0 to 90 °C. *Geochim. Cosmochim. Acta* **57**, 3533–3554.
Hendricks I. E., Duarte C. M. and Alvarez M. (2010) Vulnerability of marine biodiversity to ocean acidification: a meta-analysis. *Estuar. Coast. Shelf Sci.* **86**, 157–164.
Hillner P. E., Gratz A. J., Manne S. and Hansma P. K. (1992a) Atomic-scale imaging of calcite growth and dissolution in real time. *Geology* **20**, 359–362.
Hillner P. E., Manne S., Gratz A. J. and Hansma P. K. (1992b) AFM images of dissolution and growth on a calcite crystal. *Ultramicroscopy* **42**, 1387–1393.
Hoegh-Guldberg O., Mumby P. J., Hooten A. J., Steneck R. S., Greenfield P., Gomez E., Harvell C. D., Sale P. F., Edwards A. J. and Caldeira K. (2007) Coral reefs under rapid climate change and ocean acidification. *Science* **318**, 1737–1742.
Holcomb M., Venn A. A., Tambutte E., Tambutte S., Allemand D., Trotter J. and McCulloch M. (2014) Coral calcifying fluid pH dictates response to ocean acidification. *Sci. Rep.* **4**. http://dx.doi.org/10.1038/srep05207.
Honjo S. and Erez J. (1978) Dissolution rates of calcium carbonate in the deep ocean; an *in-situ* experiment in the North Atlantic Ocean. *Earth Planet. Sci. Lett.* **40**, 287–300.
Iglesias-Rodriguez M. D., Halloran P. R., Rickaby R. E. M., Hall I. R., Colmenero-Hidalgo E., Gittins J. R., Green D. R. H., Tyrrell T., Gibbs S. J. and von Dassow P. (2008) Phytoplankton calcification in a high-CO_2 world. *Science* **320**, 336–340.
IPCC (2013) Summary for policymakers. In *Climate Change 2013: The Physical Science Basis. Contribution of Working Group I to the Fifth Assessment Report of the Intergovernmental Panel on Climate Change* (eds. T. F. Stocker, D. Qin, G.-K. Plattner, M. Tignor, S. K. Allen, J. Boschung, A. Nauels, Y. Xia, V. Bex and P. M. Midgley). Cambridge University Press, Cambridge, United Kingdom and New York, NY, USA.
Jahnke R. A. and Jahnke D. B. (2004) Calcium carbonate dissolution in deep sea sediments: reconciling microelectrode, pore water and benthic flux chamber results. *Geochim. Cosmochim. Acta* **68**, 47–59.
Jokiel J. P. (2011) Ocean acidification and control of reef coral calcification by boundary layer limitation of proton flux. *Bull. Mar. Sci.* **87**, 639–657.
Jordan G. and Rammensee W. (1998) Dissolution rates of calcite (1014) obtained by scanning force microscopy: microtopography-based dissolution kinetics on surfaces with anisotropic step velocities. *Geochim. Cosmochim. Acta* **62**, 941–947.
Keir R. S. (1980) The dissolution kinetics of biogenic calcium carbonates in seawater. *Geochim. Cosmochim. Acta* **44**, 241–252.
Kennish M. J. and Lutz R. A. (1999) Calcium carbonate dissolution rates in deep-sea bivalve shells on the East Pacific Rise at 21 N: results of an 8-year in-situ experiment. *Palaeogeogr. Palaeoclimatol. Palaeoecol.* **154**, 293–299.
Kidwell S. M. (2001) Preservation of species abundance in marine death assemblages. *Science* **294**, 1091–1094.
Kinsey D. D. (1985) Metabolism, calcification and carbon production. I. System level studies. In *Proceedings of the 5th International Coral Reef Congress, Tahiti*, pp. 503–542.
Kleypas J. A., Buddemeier R. W., Archer D., Gattuso J.-P., Langdon C. and Opdyke B. N. (1999) Geochemical consequences of increased atmospheric carbon dioxide on coral reefs. *Science* **284**, 118–120.
Kleypas J. A., Feely R. A., Fabry V. J., Langdon C., Sabine C. L. and Robbins L. L. (2005) Impacts of ocean acidification on coral reefs and other marine calcifiers: a guide for future research (report of a workshop held), p. 18–20.
Kralj D. and Brečević L. (1995) Dissolution kinetics and solubility of calcium carbonate monohydrate. *Colloids Surf. A* **96**, 287–293.

Krief S., Hendy E. J., Fine M., Yam R., Meibom A., Foster G. L. and Shemesh A. (2010) Physiological and isotopic responses of scleractinian corals to ocean acidification. *Geochim. Cosmochim. Acta* **74**, 4988–5001.

Kroeker K. J., Kordas R. L., Crim R. N. and Singh G. G. (2010) Meta-analysis reveals negative yet variable effects of ocean acidification on marine organisms. *Ecol. Lett.* **13**, 1419–1434.

Kroeker K. J., Kordas R. L., Crim R., Hendriks I. E., Ramajo L., Singh G. S., Duarte C. M. and Gattuso J. P. (2013) Impacts of ocean acidification on marine organisms: quantifying sensitivities and interaction with warming. *Glob. Change Biol.* **19**, 1884–1896.

Kuffner I. B., Brock J. C., Grober-Dunsmore R., Hickey T. D., Bonito V., Bracone J. E. and Wright C. W. (2008) Biological communities and geomorphology of patch reefs in Biscayne National Park, Florida, USA, in Report OFR 2008–1330. *US Geological Survey*.

Lafon G. M. (1978) Equilibrium criteria for two-component solids reacting with fixed composition in an aqueous phase; example, the magnesian calcites; discussion. *Am. J. Sci.* **278**, 1455–1468.

Land L. S. (1967) Diagenesis of skeletal carbonates. *J. Sediment. Res.* **37**.

Langdon C., Takahashi T., Sweeney C., Chipman D., Goddard J., Marubini F., Aceves H., Barnett H. and Atkinson M. J. (2000) Effect of calcium carbonate saturation state on the calcification rate of an experimental coral reef. *Global Biogeochem. Cycles* **14**, 639–654.

Langdon, C., (2002) Review of experimental evidence for effects of CO_2 on calcification of reef-builders, In *Proceedings of the 9th International Coral Reef Symposium*, 1091–1098.

Lasaga A. C. and Luttge A. (2001) Variation of crystal dissolution rate based on a dissolution stepwave model. *Science* **291**, 2400–2404.

Lea A. S., Amonette J. E., Baer D. R., Liang Y. and Colton N. G. (2001) Microscopic effects of carbonate, manganese, and strontium ions on calcite dissolution. *Geochim. Cosmochim. Acta* **65**, 369–379.

Leclercq N., Gattuso J.-P. and Jaubert J. (2002) Primary production, respiration, and calcification of a coral reef mesocosm under increased CO_2 partial pressure. *Limnol. Oceanogr.* **47**, 558–564.

Lewis E. and Wallace D. W. R. (1998) *CO_2SYS: Program Developed for CO_2 System Calculations, ORNL/CDIAC-105 ed.* Carbon Dioxide Information Analysis Center, Oak Ridge National Laboratory, U.S Department of Energy, Oak Ridge, Tennessee.

Liang Y. and Baer D. R. (1997) Anisotropic dissolution at the $CaCO_3$ (1014)—water interface. *Surf. Sci.* **373**, 275–287.

Liang Y., Baer D. R., McCoy J. M., Amonette J. E. and Lafemina J. P. (1996) Dissolution kinetics at the calcite-water interface. *Geochim. Cosmochim. Acta* **60**, 4883–4887.

Liu Z. and Dreybrod W. (1997) Dissolution kinetics of calcium carbonate minerals in H_2O–CO_2 solutions in turbulent flow: the role of the diffusion boundary layer and the slow reaction $H_2O + CO_2 \rightarrow H^+ + HCO_3^-$. *Geochim. Cosmochim. Acta* **61**, 2879–2889.

Lowenstam H. A. and Abbott D. P. (1975) Vaterite: a mineralization product of the hard tissues of a marine organism (Ascidiacea). *Science* **188**, 363–365.

MacInnis I. N. and Brantley S. L. (1992) The role of dislocations and surface morphology in calcite dissolution. *Geochim. Cosmochim. Acta* **56**, 1113–1126.

MacInnis I. N. and Brantley S. L. (1993) Development of etch pit size distributions on dissolving minerals. *Chem. Geol.* **105**, 31–49.

Mackenzie F. T. and Pigott J. D. (1981) Tectonic controls of Phanerozoic sedimentary rock cycling. *J. Geol. Soc.* **138**, 183–196.

Mackenzie F. T., Bischoff W. D., Bishop F. C., Loijens M., Schoonmaker J. and Wollast R. (1983) Magnesian calcites; low-temperature occurrence, solubility and solid-solution behavior. *Rev. Mineral. Geochem.* **11**, 97–144.

McCulloch M., Trotter J., Montagna P., Falter J., Dunbar R., Freiwald A., Försterra G., López Correa M., Maier C. and Rüggeberg A., et al. (2012) Resilience of cold-water scleractinian corals to ocean acidification: boron isotopic systematics of pH and saturation state up-regulation. *Geochim. Cosmochim. Acta* **87**, 21–34.

Milliman J. D. (1978) *Dissolution of Calcium Carbonate in the Sargasso Sea (Northwest Atlantic)*. Woods Hole Oceanographic Institution.

Morse J. W. (1978) Dissolution kinetics of calcium carbonate in sea water; VI. The near-equilibrium dissolution kinetics of calcium carbonate-rich deep sea sediments. *Am. J. Sci.* **278**, 344–353.

Morse J. W. (1983) The kinetics of calcium carbonate dissolution and precipitation. *Rev. Mineral. Geochem.* **11**, 227–264.

Morse J. W. (1986) The surface chemistry of calcium carbonate minerals in natural waters: an overview. *Mar. Chem.* **20**, 91–112.

Morse J. W. and Arvidson R. S. (2002) The dissolution kinetics of major sedimentary carbonate minerals. *Earth-Sci. Rev.* **58**, 51–84.

Morse J. W. and Berner R. A. (1972) Dissolution kinetics of calcium carbonate in sea water; I, a kinetic origin for the lysocline. *Am. J. Sci.* **272**, 840–851.

Morse J. W. and Mackenzie F. T. (1990) *Geochemistry of sedimentary carbonates*. Elsevier, 706 p.

Morse J. W., de Kanel J. and Harris K. (1979) Dissolution kinetics of calcium carbonate in seawater: VII. The dissolution kinetics of synthetic aragonite and pteropod tests. *Am. J. Sci.* **279**, 488–502.

Morse J. W., Andersson A. J. and Mackenzie F. T. (2006) Initial responses of carbonate-rich shelf sediments to rising atmospheric pCO_2 and 'ocean acidification': role of high Mg-calcites. *Geochim. Cosmochim. Acta* **70**, 5814–5830.

Morse J. W., Arvidson R. S. and Lüttge A. (2007) Calcium carbonate formation and dissolution. *Chem. Rev.* **107**, 342–381.

Mucci A. (1983) The solubility of calcite and aragonite in seawater at various salinities, temperatures, and one atmosphere total pressure. *Am. J. Sci.* **283**, 780–799.

Mucci A. and Morse J. W. (1984) The solubility of calcite in seawater solutions of various magnesium concentrations, It = 0.697 m at 25 °C and one atmosphere total pressure. *Geochim. Cosmochim. Acta* **48**, 815–822.

Mucci A., Canuel R. and Zhong S. (1989) The solubility of calcite and aragonite in sulfate-free seawater and the seeded growth kinetics and composition of the precipitates at 25 °C. *Chem. Geol.* **74**, 309–320.

Nash M. C., Opdyke B. N., Troitzsch U., Russell B. D., Adey W. H., Kato A., Diaz-Pulido G., Brent C., Gardner M., Prichard J. and Kline D. I. (2013) Dolomite-rich coralline algae in reefs resist dissolution in acidified conditions. *Nat. Climate Change* **3**, 268–272.

Nestaas I. and Terjesen S. (1969) Inhibiting effect of scandium ions upon dissolution of calcium carbonate. *Acta Chem. Scand.* **23**, 2519.

Orr J. C., Fabry V. J., Aumont O., Bopp L., Doney S. C., Feely R. A., Gnanadesikan A., Gruber N., Ishida A. and Joos F. (2005) Anthropogenic ocean acidification over the twenty-first century and its impact on calcifying organisms. *Nature* **437**, 681–686.

Peterson M. N. A. (1966) Calcite: rates of dissolution in a vertical profile in the central Pacific. *Science* **154**, 1542–1544.

Pickett M. and Andersson A. J. (2015) Dissolution rates of biogenic carbonates in natural seawater at different pCO_2 conditions: a laboratory study. *Aquat. Geochem.* http://dx.doi.org/10.1007/s10498-015-9261-3.

Plath D. C., Johnson K. S. and Pytkowicz R. M. (1980) The solubility of calcite—probably containing magnesium—in seawater. *Mar. Chem.* **10**, 9–29.

Plummer L. N. and Busenberg E. (1982) The solubilities of calcite, aragonite and vaterite in CO_2–H_2O solutions between 0 and 90 °C, and an evaluation of the aqueous model for the system $CaCO_3$–CO_2–H_2O. *Geochim. Cosmochim. Acta* **46**, 1011–1040.

Plummer L. N. and Mackenzie F. T. (1974) Predicting mineral solubility from rate data; application to the dissolution of magnesian calcites. *Am. J. Sci.* **274**, 61–83.

Plummer L. and Wigley T. (1976) The dissolution of calcite in CO_2-saturated solutions at 25 °C and 1 atmosphere total pressure. *Geochim. Cosmochim. Acta* **40**, 191–201.

Plummer L. N., Wigley T. M. L. and Parkhurst D. L. (1978) The kinetics of calcite dissolution in CO_2-water systems at 5° to 60 °C and 0.0 to 1.0 atm CO_2. *Am. J. Sci.* **278**, 179–216.

Plummer L. N., Parkhurst D. L. and Wigley T. M. L. (1979) Critical review of the kinetics of calcite dissolution and precipitation, p. 537–573.

Pokrovsky O. S. and Schott J. (1999) Processes at the magnesium-bearing carbonates/solution interface: II. Kinetics and mechanism of magnesite dissolution. *Geochim. Cosmochim. Acta* **63**, 881–897.

Pokrovsky O. S. and Schott J. (2002) Surface chemistry and dissolution kinetics of divalent metal carbonates. *Environ. Sci. Technol.* **36**, 426–432.

Pokrovsky O. S., Golubev S. V. and Schott J. (2005) Dissolution kinetics of calcite, dolomite and magnesite at 25 °C and 0 to 50 atm pCO_2. *Chem. Geol.* **217**, 239–255.

Pokrovsky O. S., Golubev S. V., Schott J. and Castillo A. (2009) Calcite, dolomite and magnesite dissolution kinetics in aqueous solutions at acid to circumneutral pH, 25–150 °C and 1–55 atm pCO_2: new constraints on CO_2 sequestration in sedimentary basins. *Chem. Geol.* **265**, 20–32.

Powell E. N., Callender W. R., Staff G. M., Parsons-Hubbard K. M., Brett C. E., Walker S. E., Raymond A. and Ashton-Alcox K. A. (2008) Molluscan shell condition after eight years on the sea floor—taphonomy in the Gulf of Mexico and Bahamas. *J. Shellfish Res.* **27**, 191–225.

Raven J., Caldeira K., Elderfield H., Hoegh-Guldberg O., Liss P., Riebesell U., Shepherd J., Turley C. and Watson A. (2005) *Ocean acidification due to increasing atmospheric carbon dioxide*. The Royal Society.

Ries J. (2010) Review: geological and experimental evidence for secular variation in seawater Mg/Ca (calcite-aragonite seas) and its effects on marine biological calcification. *Biogeosciences* **7**, 2795–2849.

Ries J. (2011a) Acid ocean cover up. *Nat. Climate Change* **1**, 294–295.

Ries J. B. (2011b) Skeletal mineralogy in a high-CO_2 world. *J. Exp. Mar. Biol. Ecol.* **403**, 54–64.

Ries J. B. (2011c) A physicochemical framework for interpreting the biological calcification response to CO_2-induced ocean acidification. *Geochim. Cosmochim. Acta* **75**, 4053–4064.

Ries J. B. (2012) A sea butterfly flaps its wings. *Nat. Geosci.* **5**, 845–846.

Ries J. B., Cohen A. L. and McCorkle D. C. (2009) Marine calcifiers exhibit mixed responses to CO_2-induced ocean acidification. *Geology* **37**, 1131–1134.

Rodolfo-Metalpa R., Martin S., Ferrier-Pagès C. and Gattuso J.-P. (2010) Response of the temperate coral *Cladocora caespitosa* to mid- and long-term exposure to pCO_2 and temperature levels projected for the year 2100 AD. *Biogeosciences* **7**, 289–300.

Rodolfo-Metalpa R., Houlbrèque F., Tambutté É., Boisson F., Baggini C., Patti F. P., Jeffree R., Fine M., Foggo A. and Gattuso J. P. (2011) Coral and mollusc resistance to ocean acidification adversely affected by warming. *Nat. Climate Change* **1**, 308–312.

Roy R. N., Roy L. N., Vogel K. M., Porter-Moore C., Pearson T., Good C. E., Millero F. J. and Campbell D. M. (1993) The dissociation constants of carbonic acid in seawater at salinities 5–45 and temperatures 0 to 45 °C. *Mar. Chem.* **44**, 249–267.

Rude P. D. and Aller R. C. (1991) Fluorine mobility during early diagenesis of carbonate sediment: an indicator of mineral transformations. *Geochim. Cosmochim. Acta* **55**, 2491–2509.

Salem M. R., Mangood A. H. and Hamdona S. K. (1994) Dissolution of calcite crystals in the presence of some metal ions. *J. Mat. Sci.* **29**, 6463–6467.

Sandberg P. A. (1983) An oscillating trend in Phanerozoic non-skeletal carbonate mineralogy. *Nature* **305**, 19–22.

Schmalz R. (1965) Brucite in carbonate secreted by the red alga Goniolithon sp. *Science* **149**, 993–996.

Schott J., Brantley S., Crerar D., Guy C., Borcsik M. and Willaime C. (1989) Dissolution kinetics of strained calcite. *Geochim. Cosmochim. Acta* **53**, 373–382.

Schott J., Pokrovsky O. S. and Oelkers E. H. (2009) The link between mineral dissolution/precipitation kinetics and solution chemistry. *Rev. Mineral. Geochem.* **70**, 207–258.

Schroeder J. H. (1969) Experimental dissolution of calcium, magnesium, and strontium from recent biogenic carbonates: a model of diagenesis. *J. Sediment. Res.* **39**, 1057–1073.

Shiraki R., Rock P. A. and Casey W. H. (2000) Dissolution kinetics of calcite in 0.1 M NaCl solution at room temperature: an atomic force microscopic (AFM) study. *Aquat. Geochem.* **6**, 87–108.

Silverman J., Lazar B. and Erez J. (2007a) Community metabolism of a coral reef exposed to naturally varying dissolved inorganic nutrient loads. *Biogeochemistry* **84**, 67–82.

Silverman J., Lazar B. and Erez J. (2007b) Effect of aragonite saturation, temperature, and nutrients on the community calcification rate of a coral reef. *J. Geophys. Res.: Oceans* **112**, C05004.

Sjöberg E. L. (1976) A fundamental equation for calcite dissolution kinetics. *Geochim. Cosmochim. Acta* **40**, 441–447.

Sjöberg E. L. (1978) Kinetics and mechanism of calcite dissolution in aqueous solutions at low temperatures, 92 p.

Sjöberg E. L. and Rickard D. T. (1984) Temperature dependence of calcite dissolution kinetics between 1 and 62 °C at pH 2.7–8.4 in aqueous solutions. *Geochim. Cosmochim. Acta* **48**, 485–493.

Smith A. M., Key M. M. and Gordon D. P. (2006) Skeletal mineralogy of bryozoans: taxonomic and temporal patterns. *Earth Sci. Rev.* **78**, 287–306.

Smith A. M. (2014) Growth and calcification of marine bryozoans in a changing ocean. *Biol. Bull.* **226**, 203–210.

Suess E. (1970) Interaction of organic compounds with calcium carbonate—I. Association phenomena and geochemical implications. *Geochim. Cosmochim. Acta* **34**, 157–168.

Svensson U. and Dreybrodt W. (1992) Dissolution kinetics of natural calcite minerals in CO_2-water systems approaching calcite equilibrium. *Chem. Geol.* **100**, 129–145.

Tans P. and Keeling R. (2013) *Trends in Atmospheric Carbon Dioxide*. National Oceanic and Atmospheric Administration Earth System Research Laboratory.

Taylor P. D., James N. P., Bone Y., Kuklinski P. and Kyser T. K. (2009) Evolving mineralogy of cheilostome bryozoans. *Palaios* **24**, 440–452.

Teng H. H. (2004) Controls by saturation state on etch pit formation during calcite dissolution. *Geochim. Cosmochim. Acta* **68**, 253–262.

Teng H. H. and Dove P. M. (1997) Surface site-specific interactions of aspartate with calcite during dissolution: implications for biomineralization. *Am. Mineral.* **82**, 878–887.

Terjesen S. G., Erga O., Thorsen G. and Ve A. (1961) Phase boundary processes as rate determining steps in reactions between solids and liquids: the inhibitory action of metal ions on the formation of calcium bicarbonate by the reaction of calcite with aqueous carbon dioxide. *Chem. Eng. Sci.* **14**, 277–288.

Thorstenson D. C. and Plummer L. N. (1977) Equilibrium criteria for two-component solids reacting with fixed composition in an aqueous phase; example, the magnesian calcites. *Am. J. Sci.* **277**, 1203–1223.

Thorstenson D. and Plummer L. N. (1978) Equilibrium criteria for two-component solids reacting with fixed composition in an aqueous phase; example, the magnesian calcites; reply. *Am. J. Sci.* **278**, 1478–1488.

Tribollet A., Godinot C., Atkinson M. and Langdon C. (2009) Effects of elevated pCO_2 on dissolution of coral carbonates by microbial euendoliths. *Global Biogeochem. Cycles* **23**, GB3008. http://dx.doi.org/10.1029/2008GB003286.

Trotter J., Montagna P., McCulloch M., Silenzi S., Reynaud S., Mortimer G., Martin S., Ferrier-Pagès C., Gattuso J.-P. and Rodolfo-Metalpa R. (2011) Quantifying the pH 'vital effect' in the temperate zooxanthellate coral *Cladocora caespitosa*: validation of the boron seawater pH proxy. *Earth Planet. Sci. Lett.* **303**, 163–173.

Tynan S. and Opdyke B. N. (2011) Effects of lower surface ocean pH upon the stability of shallow water carbonate sediments. *Sci. Total Environ.* **409**, 1082–1086.

Van Cappellen P., Charlet L., Stumm W. and Wersin P. (1993) A surface complexation model of the carbonate mineral-aqueous solution interface. *Geochim. Cosmochim. Acta* **57**, 3505–3518.

Venn A., Tambutté E., Holcomb M., Allemand D. and Tambutté S. (2011) Live tissue imaging shows reef corals elevate pH under their calcifying tissue relative to seawater. *PLoS ONE* **6**, e20013.

Vinson M. D. and Lüttge A. (2005) Multiple length-scale kinetics: an integrated study of calcite dissolution rates and strontium inhibition. *Am. J. Sci.* **305**, 119–146.

Waldbusser G. G., Steenson R. A. and Green M. A. (2011) Oyster shell dissolution rates in estuarine waters: effects of pH and shell legacy. *J. Shellfish Res.* **30**, 659–669.

Walter L. M. (1985) Relative reactivity of skeletal carbonates during dissolution: implications for diagenesis. *Soc. Econ. Paleontol. Mineral. Spec. Publ.* **36**, 3–16.

Walter L. M. and Burton E. A. (1990) Dissolution of recent platform carbonate sediments in marine pore fluids. *Am. J. Sci.* **290**, 601–643.

Walter L. M. and Hanor J. S. (1979) Effect of orthophosphate on the dissolution kinetics of biogenic magnesian calcites. *Geochim. Cosmochim. Acta* **43**, 1377–1385.

Walter L. M. and Morse J. W. (1984) Reactive surface area of skeletal carbonates during dissolution: effect of grain size. *J. Sediment. Res.* **54**.

Walter L. M. and Morse J. W. (1985) The dissolution kinetics of shallow marine carbonates in seawater: a laboratory study. *Geochim. Cosmochim. Acta* **49**, 1503–1513.

Walter L. M., Bischof S. A., Patterson W. P., Lyons T. W., O'Nions R. K., Gruszczynski M., Sellwood B. W. and Coleman M. L. (1993) Dissolution and recrystallization in modern shelf carbonates: evidence from pore water and solid phase chemistry. *Philos. Trans. R. Soc. Lond. Series A: Phys. Eng. Sci.* **344**, 27–36.

Weiner S., Levi-Kalisman Y., Raz S. and Addadi L. (2003) Biologically formed amorphous calcium carbonate. *Connect. Tissue Res.* **44**, 214–218.

Weyl P. K. (1958) The solution kinetics of calcite. *J. Geol.*, 163–176.

Weyl P. K. (1965) *The Solution Kinetics of Calcite*, 428 ed. Shell Development Company, 59 p.

White A. F. and Peterson M. L. (1990) Role of reactive-surface-area characterization in geochemical kinetic models. In *ACS Symposium Series*. Oxford University Press, pp. 461–475.

Wollast R. (1990) *Rate and Mechanism of Dissolution of Carbonates in the System $CaCO_3$–$MgCO_3$, Aquatic Chemical Kinetics: Reaction Rates of Processes in Natural Waters*. John Wiley & Sons, New York, pp. 431–445.

Wollast, R. and Reinhard-Derie, D. (1977) Equilibrium and mechanism of dissolution of Mg-calcites. *The Fate of Fossil Fuel CO_2*, 479–493.

Wood H. L., Spicer J. I. and Widdicombe S. (2008) Ocean acidification may increase calcification rates, but at a cost. *Proc. R. Soc. B: Biol. Sci.* **275**, 1767–1773.

Xu J., Fan C. and Teng H. H. (2012) Calcite dissolution kinetics in view of Gibbs free energy, dislocation density, and pCO_2. *Chem. Geol.* **322**, 11–18.

Yates K. and Halley R. (2006) CO_3^{2-} concentration and pCO_2 thresholds for calcification and dissolution on the Molokai reef flat, Hawaii. *Biogeosci. Discuss.* **3**, 123–154.

Associate editor: Yair Rosenthal